Chapter 2

DYNAMICS OF MATURE TROPICAL CYCLONES

2.1 The primary and secondary circulation

The mature tropical cyclone consists of a horizontal quasi-symmetric circulation on which is superposed a thermally-direct vertical (transverse) circulation. These are sometimes referred to as the primary and secondary circulations, respectively, terms which were coined by Ooyama (1982). The combined spiralling circulation is energetically direct because the rising branch of the secondary circulation near the centre is warmer than the subsiding branch, which occurs at large radial distances (radii > 500 km). In this chapter we examine the dynamics of the spiralling circulation of tropical cyclones on the basis of the physical laws governing fluid motion and thermodynamic processes that occur. In particular we study the dynamics of a stationary axisymmetric hurricane-like vortex. In later chapters we consider the dynamics of tropical-cyclone motion and examine the asymmetric features of storms. We begin by giving an overall picture of the dynamics and then go into detail about particular important aspects.

2.2 The equations of motion

To begin with we consider the full hydrostatic equations of motion, but with the density tendency in the continuity equation omitted. The primitive equations of motion comprising the horizontal momentum equation, the hydrostatic equation, the continuity equation, the thermodynamic equation and the equation of states for frictionless motion in a rotating frame of reference on an f-plane may be expressed in cylindrical polar coordinates, (r, λ, z), as:

$$\frac{\partial u}{\partial t} + u\frac{\partial u}{\partial r} + \frac{v}{r}\frac{\partial u}{\partial \lambda} + w\frac{\partial u}{\partial z} - \frac{v^2}{r} - fv = -\frac{1}{\rho}\frac{\partial p}{\partial r}, \tag{2.1}$$

$$\frac{\partial v}{\partial t} + u\frac{\partial v}{\partial r} + \frac{v}{r}\frac{\partial v}{\partial \lambda} + w\frac{\partial v}{\partial z} + \frac{uv}{r} + fu = -\frac{1}{\rho r}\frac{\partial p}{\partial \lambda}, \tag{2.2}$$

$$\frac{\partial w}{\partial t} + u\frac{\partial w}{\partial r} + \frac{v}{r}\frac{\partial w}{\partial \lambda} + w\frac{\partial w}{\partial z} = -\frac{1}{\rho}\frac{\partial p}{\partial z} - g, \tag{2.3}$$

$$\frac{1}{r}\frac{\partial \rho r u}{\partial r} + \frac{1}{r}\frac{\partial \rho v}{\partial \lambda} + \frac{\partial \rho w}{\partial z} = 0, \tag{2.4}$$

$$\frac{\partial \theta}{\partial t} + u\frac{\partial \theta}{\partial r} + \frac{v}{r}\frac{\partial \theta}{\partial \lambda} + w\frac{\partial \theta}{\partial z} = \dot{\theta} \tag{2.5}$$

$$\rho = p_* \pi^{\frac{1}{\kappa}-1}/(R\theta) \tag{2.6}$$

where (u, v, w) is the velocity vector in component form, ρ is the air density, f is the Coriolis parameter, p is the pressure, θ is the potential temperature $\dot{\theta}$ is the diabatic heating rate, $\pi = (p/p_*)^\kappa$ is the Exner function, R is the specific gas constant, $\kappa = R/c_p$, c_p is the specific heat at constant pressure, and $p_* = 1000$ mb. The temperature is defined by $T = \pi\theta$. For tropical-cyclone scale motions it is a good approximation to make the hydrostatic approximation, whereupon Eq. (2.3) reduces to

$$\frac{\partial p}{\partial z} = -\rho g. \tag{2.7}$$

Multiplication of Eq. (2.2) by r and a little manipulation leads to the equation

$$\frac{\partial M}{\partial t} + u\frac{\partial M}{\partial r} + \frac{v}{r}\frac{\partial M}{\partial \lambda} + w\frac{\partial M}{\partial z} = -\frac{1}{\rho}\frac{\partial p}{\partial \lambda}, \tag{2.8}$$

where

$$M = rv + \frac{1}{2}r^2 f, \tag{2.9}$$

is the absolute angular momentum per unit mass of an air parcel about the rotation axis. If the flow is axisymmetric (and frictionless), the right-hand-side of (2.8) is zero and the absolute angular momentum is conserved.

Exercise 2.1 Assuming the most general form of the mass conservation equation:

$$\frac{\partial \rho}{\partial t} + \frac{1}{r}\frac{\partial(\rho r u)}{\partial r} + \frac{1}{r}\frac{\partial(\rho v)}{\partial \lambda} + \frac{\partial(\rho w)}{\partial z} = 0,$$

show that the absolute angular momentum per unit volume,

$$M_v = \rho\left(rv + \frac{1}{2}r^2 f\right),$$

satisfies the equation:

$$\frac{\partial M_v}{\partial t} + \frac{1}{r}\frac{\partial(r u M_v)}{\partial r} + \frac{1}{r}\frac{\partial(v M_v)}{\partial \lambda} + \frac{\partial(w M_v)}{\partial z} = -\frac{\partial p}{\partial \lambda}.$$

2.3 Buoyancy

The buoyancy of an air parcel in a density-stratified air layer is defined as the difference between the weight of air displaced by the parcel (the upward thrust according to Archimedes principle) and the weight of the parcel itself. This quantity is normally expressed per unit mass of the air parcel under consideration, i.e.

$$b = -g\frac{(\rho - \rho_a)}{\rho}, \tag{2.10}$$

where ρ is the density of the parcel, $\rho_a = \rho_a(z)$ is the density of the environment at the same height z as the parcel, and g is the acceleration due to gravity. Here and elsewhere the vertical coordinate z is defined to increase in the direction opposite to gravity. The calculation of the upward thrust assumes that the pressure within the air parcel is the same as that of its environment *at the same level*, an assumption that may be unjustified in a rapidly-rotating vortex. In the latter case one can define a generalized buoyancy force, which acts normal to the isobaric surface intersecting the air parcel and which is proportional to the density difference between the parcel and its environment along that surface (see below).

A similar expression for the buoyancy force given in (2.10) may be obtained by starting from the vertical momentum equation and replacing the pressure p by the sum of a reference pressure p_{ref} and a perturbation pressure, p'. The former is taken to be in hydrostatic balance with a prescribed reference density ρ_{ref}, which is often taken, for example, as the density profile in the environment. In real situations, the environmental density is not uniquely defined, but could be taken as the horizontally-averaged density over some large domain surrounding the air parcel. Neglecting frictional forces, the vertical acceleration per unit mass can be written alternatively as

$$\frac{Dw}{Dt} = -\frac{1}{\rho}\frac{\partial p}{\partial z} - g \text{ or, } \frac{Dw}{Dt} = -\frac{1}{\rho}\frac{\partial p'}{\partial z} + b \tag{2.11}$$

where w is the vertical velocity, D/Dt is the material derivative, and t is the time presents a similar derivation, but makes the anelastic approximation (Ogura and Phillips, 1962), in which the density in the denominator of (2.10) is approximated by that in the environment. Clearly, the sum of the vertical pressure gradient and gravitational force per unit mass acting on an air parcel is equal to the sum of the vertical gradient of perturbation pressure and the buoyancy force, where the latter is calculated from Eq. (2.10) *by comparing densities at constant height*. The expression for b in (2.11) has the same form as that in (2.10), but with ρ_{ref} in place of ρ_a. However, the derivation circumvents the need to assume that the local (parcel) pressure equals the environmental pressure when calculating b. The foregoing decomposition indicates that, in general, the buoyancy force is not uniquely defined because it depends on the (arbitrary) choice of a reference density. However, the sum of the buoyancy force and the perturbation pressure gradient per unit mass *is* unique. If the motion is hydrostatic, the perturbation pressure gradient and the buoyancy force are equal and opposite, but they remain non-unique.

Using the gas law ($p = \rho RT$, where R is the specific gas constant) and the usual definition of virtual potential temperature, the buoyancy force per unit mass can be written as

$$b = g\left[\frac{(\theta - \theta_{ref})}{\theta_{ref}} - (\kappa - 1)\frac{p'}{p_{ref}}\right], \tag{2.12}$$

where θ is the virtual potential temperature of the air parcel in K and θ_{ref} is the corresponding reference value. The second term on the right-hand-side of (2.12) is sometimes referred to as the "dynamic buoyancy", but in some sense this is a misnomer since buoyancy depends fundamentally on the density perturbation and this term simply corrects the calculation of the density perturbation based on the virtual potential temperature perturbation. If the perturbation pressure gradient terms in (2.11) are written in terms of the Exner function and/or its perturbation, the second term in (2.12) does not appear in the expression for buoyancy. The expression (2.12) is valid also in a rapidly rotating vortex, but as shown in section 2.5, there exists then a radial component of buoyancy as well. When clouds are involved it may be advantageous to include the drag of hydrometeors in the definition of buoyancy, but we omit this additional effect here.

2.4 The primary circulation

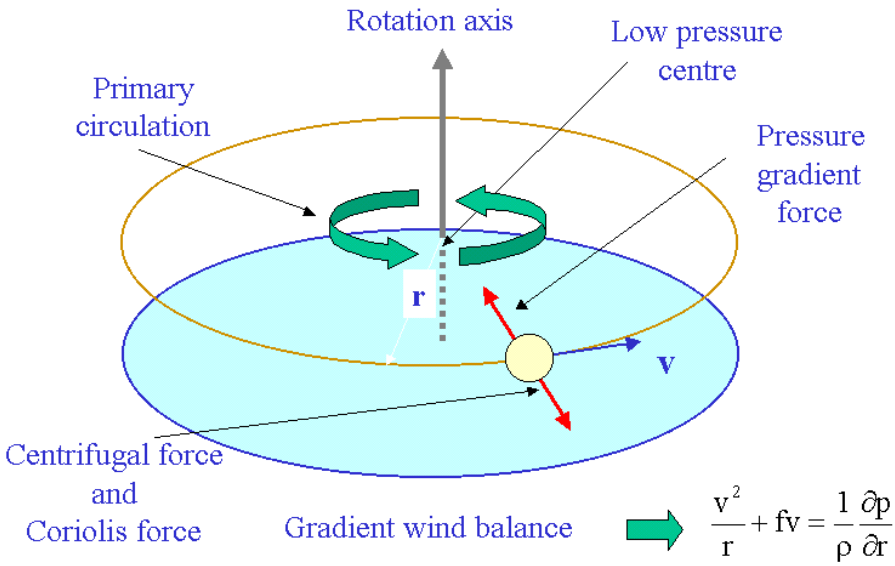

Figure 2.1: Schematic diagram illustrating the gradient wind force balance in the primary circulation of a tropical cyclone.

To begin with we assume that the flow is steady ($\partial/\partial t \equiv 0$) and we ignore the secondary circulation, i.e. we assume that the radial velocity is identically zero (see

Fig. 2.1). Then Eq. (2.1) reduces to the *gradient wind equation*:

$$\frac{v^2}{r} + fv = \frac{1}{\rho}\frac{\partial p}{\partial r}. \tag{2.13}$$

In the data for Hurricane Gilbert shown in Fig. 1.11b, the strongest radial gradient of the 700 mb geopotential height roughly coincides with the maximum swirling wind, which suggests that the wind may be in gradient balance with the mass field. In fact gradient balance prevailed in the mid-troposphere in Gilbert to within a root-mean-squared deviation of ± 4m s^{-1} (Willoughby, 1995, p28).

Taking $(\partial/\partial z)[\rho\times$ Eq. (2.13)] and $(\partial/\partial r)$[Eq. (2.2)] and eliminating the pressure we obtain the *thermal wind equation*

$$g\frac{\partial(\ln\rho)}{\partial r} + C\frac{\partial(\ln\rho)}{\partial z} = -\frac{\partial C}{\partial z}. \tag{2.14}$$

where we have defined

$$C = \frac{v^2}{r} + fv \tag{2.15}$$

to represent the sum of the centrifugal and Coriolis forces per unit mass. This is a linear first-order partial differential equation for $\ln\rho$. The characteristics of the equation satisfy

$$\frac{dz}{dr} = \frac{C}{g}. \tag{2.16}$$

The characteristics are just the isobaric surfaces, because a small displacement (dr, dz) along an isobaric surface satisfies $(\partial p/\partial r)dr+(\partial p/\partial z)dz = 0$. Using the equations for hydrostatic balance, $\partial p/\partial z = -g\rho$, and gradient wind balance, $\partial p/\partial r = C\rho$, gives the equation for the characteristics. Alternatively, note that the pressure gradient per unit mass, $(1/\rho)(\partial p/\partial r, 0, \partial p/\partial z) = (C, 0, -g)$, which defines the "generalized gravity", $\mathbf{g_e}$; see Fig. 2.2. The density variation along the characteristics is governed by the equation

$$\frac{d}{dr}\ln\left(\frac{\rho}{\rho_a}\right) = -\frac{1}{g}\frac{\partial C}{\partial z}. \tag{2.17}$$

Given the vertical density profile, $\rho_a(z)$, these Eqs. (2.16) and (2.17) can be integrated inwards along the isobars to obtain the balanced axisymmetric density and pressure distributions. Thus Eq. (2.16) gives the height of the pressure surface that has the value $p_a(z)$, say, at radius R.

It follows from (2.17) that for a barotropic vortex ($\partial v/\partial z = 0$), ρ is constant along an isobaric surface, i.e. $\rho = \rho(p)$, whereupon T_v is a constant also. Note that $\partial C/\partial z = (2v/r + f)(\partial v/\partial z)$.

The thermal wind equation (2.14) or (2.17) shows also that for a cyclonic vortex ($v > 0$) with $dv/dz < 0$, $\log(\rho/\rho_a)$ and hence ρ decrease with decreasing radius along the isobaric surface so that the virtual temperature $T_v(r, z)$ and θ increase. Thus the vortex is warm cored. Conversely, if $dv/dz > 0$, the vortex is cold cored. Certainly

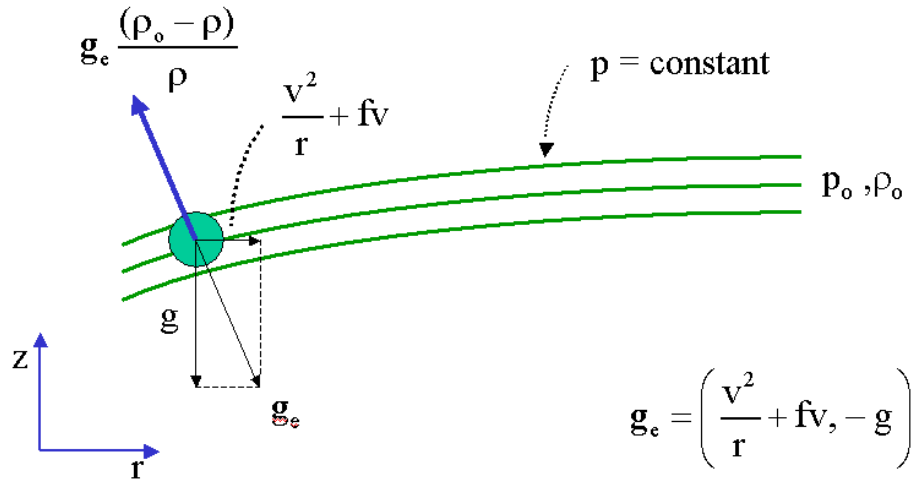

Figure 2.2: Schematic radial-height cross-section of isobaric surfaces in a rapidly-rotating vortex showing the forces on an air parcel including the gravitational force g, per unit mass, and the sum of the centrifugal and Coriolis forces $C = v^2/r + fv$ per unit mass. Note that the isobaric surfaces are normal to the local "generalized gravitational force" $\mathbf{g_e} = (C, 0, -g)$. The Archimedes force $-\mathbf{g_e}\rho_{ref}$ slopes upwards and inwards while the weight $\mathbf{g_e}\rho$ slopes downwards and outwards. Thus the net buoyancy force acting on the parcel per unit mass is $|\mathbf{g_e}|(\rho_{ref} - \rho)/\rho$ in the direction shown.

Eq. (2.14) *is consistent with* the observation that tropical cyclones are warm-cored systems (i.e. $\partial T_v/\partial r < 0$), and that the tangential wind speed decreases with altitude ($\partial v/\partial z < 0$). Note that on account of Eq. (2.16), the characteristics dip down as the axis is approached. The reason for the warm core structure is discussed in section 2.5.

The analysis above shows that any steady vortical flow with velocity field $\mathbf{u} = (0, v(r, z), 0)$ is a solution of the basic equation set (2.1) - (2.6), when the density field satisfies (2.14). Willoughby (1990) has shown from observations that the primary circulation of a hurricane is approximately in gradient wind balance so the foregoing analysis is a good start in understanding the structure of this circulation. However the solution neglects the secondary circulation associated with nonzero u and w and it neglects the effects of friction near the sea surface. These are topics of subsequent subsections.

Exercise 2.2 Show that in terms of the Exner function, Eqs. (2.13) and (2.7) may be written as

$$\chi C = c_p \frac{\partial \pi}{\partial r} \quad \text{and} \quad -\chi g = c_p \frac{\partial \pi}{\partial z}, \tag{2.18}$$

respectively.

Exercise 2.3 Show that Eq. (2.14) may be reformulated as

$$g\frac{\partial(\ln\chi)}{\partial r} + C\frac{\partial(\ln\chi)}{\partial z} = -\frac{\partial C}{\partial z}. \tag{2.19}$$

where $\chi = 1/\theta$.

It is instructive to compare the magnitude of the centrifugal and Coriolis terms in Eq. (2.1), their ratio being

$$Ro(r) = \frac{v}{fr}. \tag{2.20}$$

This equation defines a local Rossby number for the flow. At the radius of maximum tangential wind speed, r_m, the tangential wind speed at this radius, v_m, *Ro* is typically on the order of $40 \div (40 \times 10^3 \times 5 \times 10^{-5}) = 20$, typical values for r_m and v_m being 40 km and 40 m s^{-1}, respectively. It follows that the inner core region of a tropical cyclone is approximately in *cyclostrophic balance*, i.e. the Coriolis forces are relatively small. However, at a radius of 200 km, where the wind speeds may be on the order of 10 m s^{-1}, $Ro \approx 1$ and Coriolis forces are comparable with centrifugal forces. As the radius increases further, the circulation becomes more and more *geostrophic*, i.e. *Ro* becomes small compared with unity.

2.5 Generalized buoyancy

In a rapidly-rotating, axisymmetric vortex, an air parcel experiences not only the gravitational force, but also the radial force $C = v^2/r + fv$, where v is the tangential wind component at radius r. If the vortex is in hydrostatic and gradient wind balance, the isobaric surfaces slope in the vertical and are normal to the effective gravity, $\mathbf{g_e} = (C, 0, -g)$, expressed in cylindrical coordinates (r, λ, z) (see Fig. 2.2). The Archimedes force acting on the parcel is then $-\mathbf{g_e}\rho_{ref}$ and the effective weight of the parcel is $\mathbf{g_e}\rho$, where ρ_{ref} is now the far-field (reference-) density *along the same isobaric surface as the parcel*. Accordingly, we may define a *generalized buoyancy force per unit mass*:

$$\mathbf{b} = \mathbf{g_e}\frac{\rho - \rho_{\mathbf{ref}}}{\rho}, \tag{2.21}$$

analogous to the derivation of (2.10). Note that unless $v(v + rf) < 0$, fluid parcels that are lighter than their environment have an inward-directed component of generalized buoyancy force as well as an upward component, while heavier parcels have an outward component as well as a downward component. This result provides the theoretical background for a *centrifuge*.

2.6 The tropical-cyclone boundary layer

It turns out that the effects of surface friction in a tropical cyclone have a dramatic influence not only on the flow in the layer where friction acts, the so-called boundary layer, but also on the flow above this layer. The boundary layer is typically about 500 m deep. One obvious effect of friction is to reduce the tangential wind speed near the surface. However, a scale analysis shows that it has little effect on the pressure field so that the radial pressure gradient in the boundary layer is approximately the same as that immediately above the layer (see e.g. Smith 1968). However, the centrifugal and Coriolis forces are reduced by friction leaving a *net* inward force on air parcels within the boundary layer, which leads to inflow within the layer (Fig. 2.3). Far from the rotation axis, both the inflow velocity and the radial mass flux increase with decreasing radius and this leads to *forced* subsidence above the boundary layer. At inner radii, where the inflow and mass flux begin to decline, air is discharged from the boundary layer into the vortex above. In other words, the presence of the boundary layer *forces* vertical motion in the vortex above the boundary layer. In the tropical cyclone, the air in the boundary layer is moistened as it spirals inwards over the warm ocean. The moistening elevates the pseudo-equivalent potential temperature of the boundary-layer air, θ_{eb}, so that $\partial\theta_{eb}/\partial r < 0$. We consider now the fate of this moist air and return in section 2.9 to examine in detail the dynamics and thermodynamics of the boundary layer. There we show that given the tangential wind speed distribution for a steady axisymmetric vortex, one can determine the radial distribution of the vertically-averaged wind speed components in the boundary layer as functions of radius as well as the induced vertical velocity at the top of the boundary layer. Given also the vertically-averaged temperature and specific humidity at some large radius and the sea surface temperature beneath the vortex, one can determine the radial variation of the vertically-averaged θ_{eb} in the boundary layer.

2.7 Moist convection and the sloping eyewall

When the inward-spiralling moisture-laden air is forced upwards out of the boundary layer in the inner core region, it expands and cools and condensation rapidly occurs. As the air continues to rise in the eyewall clouds, latent heat is released and a significant fraction of the condensed water falls out of the clouds as precipitation. The latent heat release is responsible for the warm core in the cyclone, but only a small fraction of the heat released appears as an elevated temperature perturbation at a particular height; most of it is balanced by the adiabatic cooling that occurs as air parcels continue to rise and expand. We may think of the effect on the temperature field as follows. To a first approximation, ascending air parcels conserve their θ_e as indicated in Fig. 2.4. Since the air in the eyewall clouds is saturated, the virtual temperature of an air parcel at a particular pressure level is a monotonically-increasing function of its θ_e, which, in turn, is equal to the θ_e it had when it left the boundary layer. Therefore, at least in the eyewall cloud region the

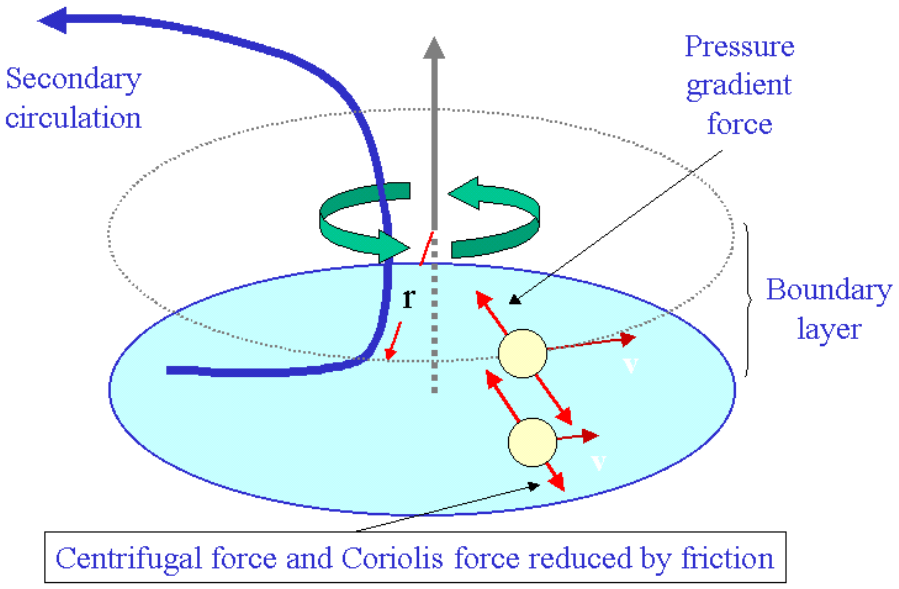

Figure 2.3: Schematic diagram illustrating the disruption of gradient wind balance by friction in the boundary layer leaving a net inward pressure gradient that drives the secondary circulation with inflow in the boundary layer and outflow above it.

radial gradient of $T_v(p)$ is determined by the radial gradient of θ_e at the top of the boundary layer, which as noted above is negative. In other words, at any level in the cloudy region, $(\partial T_v/\partial r)_p < 0$, which explains why the tropical cyclone has a warm core outside the eye. The reason that the eye is warm also is discussed in the next section. The discussion in section 2.4 indicates that the boundary layer in a mature hurricane controls not only the rate at which air ascends at a particular radius, but determines also the radial gradient of virtual temperature (and hence density) above the boundary layer, at least in regions of ascent.

From mass continuity, the air that converges in the boundary layer must flow outwards above the boundary layer, a fact that accounts for the outward slope of the eyewall and of air parcel trajectories. Ascending air parcels approximately conserve their absolute angular momentum, M, as well as their θ_e so that (absolute) angular momentum surfaces and the moist isentropes are approximately coincident (at least where there is cloud) and these surfaces slope outwards with height as indicated schematically in Fig. 2.4.

2.8 The tropical cyclone eye

As we have seen, the eye is a cloud free region surrounding the storm axis where the air temperature is warmest. Therefore, it would be reasonable to surmise that the air within it has undergone descent during the formative stages of the cyclone, and that

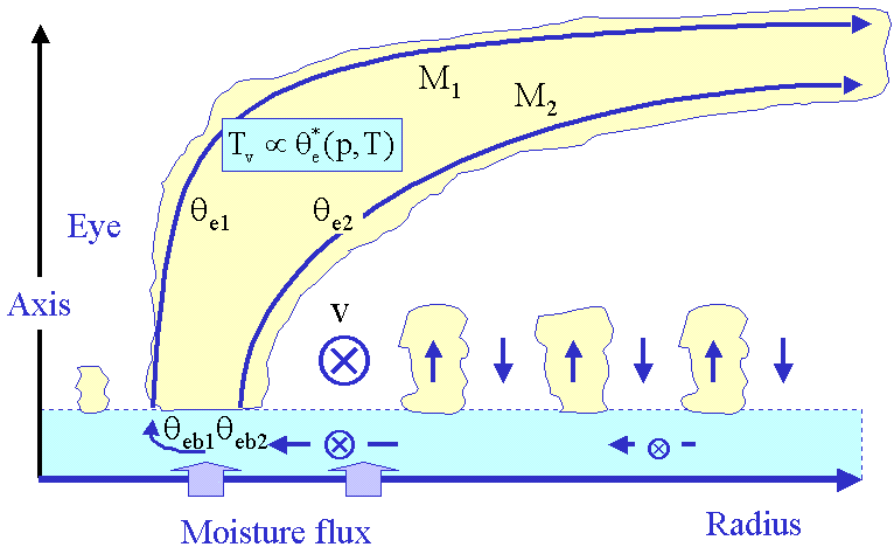

Figure 2.4: Schematic diagram of the secondary circulation of a mature tropical cyclone showing the eye and the eyewall clouds. Air spirals inwards in a shallow boundary layer near the sea surface, picking up moisture as it does so. The absolute angular momentum, M, and equivalent potential temperature, θ_e of an air parcel is conserved after the parcel leaves the boundary layer and ascends in the eyewall clouds. The precise values of these quantities depend on the radius at which the parcel exits the boundary layer. At radii beyond the eyewall cloud, shallow convection plays an important role in moistening and cooling the lower troposphere above the boundary layer and warming and drying the boundary layer as indicated.

possibly it continues to descend. The question then is: why doesn't the inflowing air spiral in as far as the axis of rotation. We address this question later, but first note that eye formation is consistent with other observed features of the tropical cyclone circulation. The following discussion is based on that of Smith (1980). Assuming that the primary circulation is in gradient wind balance, we may integrate Eq. (2.13) with radius to obtain a relationship between the pressure perturbation at a given height z on the axis to the tangential wind field distribution, i.e:

$$p(0,z) = p(\infty,z) - \int_0^\infty \rho(\frac{v^2}{r} + fv)dr, \tag{2.22}$$

where $p(\infty,z)$ is the environmental pressure at the same height. Differentiating Eq. (2.22) with respect to height and dividing by the density gives the perturbation pressure gradient per unit mass along the vortex axis:

$$-\frac{1}{\rho}\frac{\partial(p-p_\infty)}{\partial z} = -\frac{1}{\rho}\frac{\partial}{\partial z}\int_0^\infty \rho(\frac{v^2}{r} + fv)dr. \tag{2.23}$$

Observations in tropical cyclones show that the tangential wind speed decreases

with height above the boundary layer and that the vortex widens with height in the sense that the radius of the maximum tangential wind speed increases with height (see Fig. 1.11). This behaviour, which is consistent with outward-slanting absolute angular momentum surfaces as discussed above, implies that the integral on the right-hand-side of Eq. (2.23) decreases with height. Then Eq. (2.23) shows that there must be a downward-directed perturbation pressure gradient force along the vortex axis. This perturbation pressure gradient tends to drive subsidence along and near to the axis to form the eye. However, as this air subsides, it is compressed and warms relative to air at the same level outside the eye and thereby becomes locally buoyant (i.e. relative to the air outside the eye). This upward buoyancy approximately balances the downward directed (perturbation) pressure gradient so that the actual subsidence results from a small residual force. In essence the flow remains close to hydrostatic balance.

As the vortex strengthens, the downward pressure gradient must increase and the residual force must be downwards to drive further subsidence. On the other hand, if the vortex weakens, the residual force must be upwards, allowing the air to re-ascend. In the steady state, the residual force must be zero and there is no longer a need for up- or down motion in the eye, although, in reality there may be motion in the eye associated with turbulent mixing across the eyewall or with asymmetric instabilities within the eye.

It is not possible to measure the vertical velocity that occur in the eye, but one can make certain inferences about the origin of air parcels in the eye from their thermodynamic characteristics, which can be measured (see e.g. Willoughby, 1995).Note that $\partial T/\partial p)_{s*}$ is just the temperature lapse rate as a function of pressure along a moist adiabat.

2.9 A model for the boundary layer

We consider now a simple model for the tropical cyclone boundary layer as described by Smith (2003). The boundary layer equations for a steady axisymmetric vortex in a homogeneous fluid on an f-plane are:

$$\frac{1}{r}\frac{\partial}{\partial r}(ru^2) + \frac{\partial}{\partial z}(uw) + \frac{v_{gr}^2 - v^2}{r} + f(v_{gr} - v) = \frac{\partial}{\partial z}\left(K\frac{\partial u}{\partial z}\right), \tag{2.24}$$

$$\frac{1}{r^2}\frac{\partial}{\partial r}(r^2uv) + \frac{\partial}{\partial z}(vw) + fu = \frac{\partial}{\partial z}\left(K\frac{\partial v}{\partial z}\right), \tag{2.25}$$

$$\frac{1}{r}\frac{\partial}{\partial r}(ru\varphi) + \frac{\partial}{\partial z}(w\varphi) = \frac{\partial}{\partial z}\left(K\frac{\partial \varphi}{\partial z}\right), \tag{2.26}$$

$$\frac{\partial}{\partial r}(ru) + \frac{\partial}{\partial z}(rw) = 0, \tag{2.27}$$

where (u, v, w) is again the velocity vector in a stationary cylindrical coordinate system (r, ϕ, z), $v_{gr}(r)$ is the tangential wind speed at the top of the boundary layer, φ is a scalar quantity, taken here to be the dry static energy or the specific humidity, and K is an eddy diffusivity, which we assume here to be the same for momentum, heat and moisture. Let us assume that condensation does not occur in the boundary layer: we can check that saturation does not arise in the calculations. Taking the integral of Eqs. (2.24) - (2.27) with respect to z from $z = 0$ to the top of the boundary layer, $z = \delta$, and assuming that δ is a constant, we obtain:

$$\frac{d}{dr}(r\int_0^\delta u^2 dz) + [ruw]|_{z=\delta} + \int_0^\delta (v_{gr}^2 - v^2)dz + rf\int_0^\delta (v_{gr} - v)dz = -Kr\left.\frac{\partial u}{\partial z}\right|_{z=0}, \tag{2.28}$$

$$\frac{d}{dr}(r^2\int_0^\delta uvdz) + [r^2vw]\big|_{z=\delta} + fr^2\int_0^\delta udz = -Kr^2\left.\frac{\partial v}{\partial z}\right|_{z=0}, \tag{2.29}$$

$$\frac{d}{dr}(r\int_0^\delta u\varphi dz) + [rw\varphi]|_{z=\delta} = -Kr\left.\frac{\partial \varphi}{\partial z}\right|_{z=0}, \tag{2.30}$$

$$\frac{d}{dr}\int_0^\delta rudz + [rw]|_{z=\delta} = 0. \tag{2.31}$$

Now

$$[ruw]_{z=\delta} = ru_b w_{\delta_+} + ru_{gr} w_{\delta_-},$$

where u_{gr} is the radial component of flow above the boundary layer, taken here to be zero, $w_{\delta_+} = \frac{1}{2}(w_\delta + |w_\delta|)$, and $w_{\delta-} = \frac{1}{2}(w_\delta - |w_\delta|)$. Note that w_{δ_+} is equal to w_δ if the latter is positive and zero otherwise, while w_{δ_-} is equal to w_δ if the latter is negative and zero otherwise. The assumption that δ is a constant may have to be reassessed later, but allowing it to vary with radius precludes the relatively simple approach that follows. A bulk drag law is assumed to apply at the surface:

$$K\left.\frac{\partial \mathbf{u}}{\partial z}\right|_{z=0} = C_D|\mathbf{u_b}|\mathbf{u_b},$$

where C_D is a drag coefficient and $\mathbf{u_b} = (u_b, v_b)$. Here u_b and v_b denote the values of u and v in the boundary layer, which are assumed to be independent of depth. A similar law is taken for φ:

$$K\left.\frac{\partial \varphi}{\partial z}\right|_{z=0} = C_\varphi|\mathbf{u_b}|(\varphi_b - \varphi_s),$$

where φ_b and φ_s are the values of φ in the boundary layer and at the sea surface, respectively. In the case of temperature φ_s is the sea surface temperature and in the case of moisture it is the saturation specific humidity at this temperature. Following Shapiro (1983, p1987) we use the formula $C_D = C_{D0} + C_{D1}|\mathbf{u_b}|$, where $C_{D0} =$

1.1×10^{-3} and $C_{D1} = 4 \times 10^{-5}$. Further, we assume here that $C_\varphi = C_D$, although there is mounting evidence that they are not the same and that neither continue to increase linearly with wind speed at speeds in excess of, perhaps, 25 m s^{-1} (Emanuel, 1995b).

Carrying out the integrals in Eqs. (2.28) - (2.31) and dividing by δ gives

$$\frac{d}{dr}(ru_b^2) = -\frac{w_{\delta+}}{\delta} ru_b - (v_{gr}^2 - v_b^2) - rf(v_{gr} - v_b) - \frac{C_D}{\delta} r(u_b^2 + v_b^2)^{1/2} u_b, \tag{2.32}$$

$$\frac{d}{dr}(ru_b rv_b) = -r\frac{w_{\delta+}}{\delta} rv_b - r\frac{w_{\delta-}}{\delta} rv_{gr} - r^2 fu_b - \frac{C_D}{\delta} r^2 (u_b^2 + v_b^2)^{1/2} v_b, \tag{2.33}$$

$$\frac{d}{dr}(ru_b\varphi_b) = -\frac{w_{\delta+}}{\delta} r\varphi_b - r\frac{w_{\delta-}}{\delta}\varphi_{\delta+} + \frac{C_\varphi}{\delta} r(u_b^2 + v_b^2)^{1/2}(\varphi_s - \varphi_b), \tag{2.34}$$

and

$$\frac{d}{dr}(ru_b) = -r\frac{w_\delta}{\delta}, \tag{2.35}$$

which may be written

$$\frac{du_b}{dr} = -\frac{w_\delta}{\delta} - \frac{u_b}{r}. \tag{2.36}$$

Moreover, for any dependent variable η

$$\frac{d}{dr}(ru_b\eta) = ru_b\frac{d\eta}{dr} + \eta\frac{d}{dr}(ru_b) = ru_b\frac{d\eta}{dr} - \frac{w_\delta}{\delta} r\eta,$$

where η is either u_b, v_b or φ_b. Then Eqs. (2.32) and (2.33) become

$$u_b\frac{du_b}{dr} = u_b\frac{w_{\delta-}}{\delta} - \frac{(v_{gr}^2 - v_b^2)}{r} - f(v_{gr} - v_b) - \frac{C_D}{\delta}(u_b^2 + v_b^2)^{1/2} u_b, \tag{2.37}$$

$$u_b\frac{dv_b}{dr} = \frac{w_{\delta-}}{\delta}(v_b - v_{gr}) - (\frac{v_b}{r} + f)u_b - \frac{C_D}{\delta}(u_b^2 + v_b^2)^{1/2} v_b. \tag{2.38}$$

Equation (2.34) becomes

$$u_b\frac{d\varphi_b}{dr} = \frac{w_{\delta-}}{\delta}(\varphi_b - \varphi_{\delta+}) + \frac{C_\varphi}{\delta}(u_b^2 + v_b^2)^{1/2}(\varphi_s - \varphi_b) - R_b, \tag{2.39}$$

where $\varphi_{\delta+}$ is the value of φ just above the boundary layer. The term $-R_b$ is added to the equation when φ is the dry static energy and represents the effects of radiative cooling, respectively.

Equations (2.37) - (2.39) form a system that may be integrated radially inward from some large radius R to find u_b, v_b, φ_b and w_δ as functions of r, given values of

these quantities at $r = R$. First Eq. (2.37) must be modified using (2.36) to give an expression for w_δ. Combining[1] these two equations gives

$$w_\delta = \frac{\delta}{1+\alpha}\left[\frac{1}{u_b}\left\{\frac{(v_{gr}^2 - v_b^2)}{r} + f(v_{gr} - v_b) + \frac{C_D}{\delta}(u_b^2 + v_b^2)^{1/2}u_b\right\} - \frac{u_b}{r}\right], \qquad (2.40)$$

where α is zero if the expression in square brackets is negative and unity if it is positive.

2.9.1 Shallow convection

An important feature of the convective boundary layer (CBL) over the tropical oceans in regions of large-scale subsidence is the near ubiquity of shallow convection. Such regions include the outer region of hurricanes. Shallow convection plays an important role in the exchange of heat and moisture between the subcloud layer, the layer modelled in this paper, and the cloudy layer above. Excellent reviews of the CBL structure are given by Emanuel (1994, Chapter 13) and Betts (1997). Over much of the tropical Pacific Ocean, for example, in regions of subsidence, the subcloud layer is typically 500 m deep and is well-mixed, with relatively uniform vertical profiles of potential temperature, specific humidity and dry or moist static energy. The cloudy layer is capped by an inversion at an altitude of about 800 mb. A similar structure was found in the outer region of Hurricane Eloise (1975) by Moss and Merceret (1976), the mixed layer depth being about 650 m in this case. The clouds, known as tradewind cumuli, are widely spaced and have their roots in the subcloud layer. They generally don't precipitate, but evaporate into the dry subsiding air that penetrates the inversion, thereby moistening and cooling the subcloud layer. In turn, the compensating subsidence in the environment of clouds transports potentially warm and dry air into the subcloud layer. This drying opposes the moistening of the subcloud layer by surface fluxes, keeping its relative humidity at values around 80 %. The equilibrium state of the CBL, including its depth and that of the subcloud layer, is governed primarily by radiative cooling, subsidence, convective transports, and surface latent and sensible heat fluxes (Emanuel, *op. cit.*, Betts, *op. cit.*). Modelling the subcloud layer requires a knowledge of the cloud-base mass flux, which together with the large-scale subsidence, determines the rate at which cloud layer air enters the subcloud layer. Emanuel (1989) used a simple cloud model to determine the mass flux of shallow convection, while Zhu and Smith (2002) use the closure scheme of Arakawa (1969), in which the mass flux is assumed to be proportional

[1]Eq. (2.37) is written in the form

$$u_b\frac{w_{\delta_-}}{\delta} = u_b\frac{du_b}{dr} + \{...\} \quad \text{and} \quad \frac{du_b}{dr}$$

is eliminated from this expression using (2.36). Note that if $w_\delta < 0$, $w_\delta = w_{\delta_-}$, in which case $\alpha = 1$. If $w_\delta > 0$, $w_{\delta_-} = 0$, in which case $\alpha = 0$.

to the degree of convective instability between the subcloud layer and that above. As we do not predict the thermodynamic variables represented by $\varphi_{\delta+}$ above the boundary layer in this simple model, we simply choose a constant value for the mass flux of shallow convection, w_{sc}, and add this to $w_{\delta-}$ in Eqs. (2.37) - (2.39) (even if $w_{\delta-} = 0$). However, w_δ in Eq. (2.32) is left unchanged as shallow convection does not cause a *net* exchange of mass between the cloud and subcloud layers. The value for w_{sc} is chosen to ensure that the thermodynamic profile at large radius is close to radiative-convective equilibrium (see section 5).

2.9.2 Starting conditions at large radius

We assume that the flow above the boundary layer is in approximate geostrophic balance at large radii where the boundary layer is essentially governed by Ekman-like dynamics. Specifically we assume that at $r = R$, far from the axis of rotation, the flow above the boundary layer is steady and in *geostrophic* balance with tangential wind $v_{gr}(R)$. In addition we take C_D to be a constant equal to $C_{D0} + C_{D1} v_{gr}(R)^2$. Then u_b and v_b satisfy the equations:

$$f(v_{gr} - v_b) = -\frac{C_D}{\delta}(u_b^2 + v_b^2)^{1/2} u_b, \tag{2.41}$$

$$f u_b = -\frac{C_D}{\delta}(u_b^2 + v_b^2)^{1/2} v_b. \tag{2.42}$$

Let $(u_b, v_b) = v_{gr}(u', v')$ and $\Lambda = f\delta/(C_D v_{gr})$. Then equations (2.41) and (2.42) become

$$\Lambda(1 - v') = -(u'^2 + v'^2)^{1/2} u', \tag{2.43}$$

and

$$\Lambda u' = -(u'^2 + v'^2)^{1/2} y. \tag{2.44}$$

The last two equations have the solution

$$v' = -\frac{1}{2}\Lambda^2 + (\frac{1}{4}\Lambda^4 + \Lambda^2)^{1/2}. \tag{2.45}$$

and

$$u' = -[(1 - v')v']^{1/2}, \tag{2.46}$$

whereupon u_b and v_b follow immediately on multiplication by v_{gr}. The vertical velocity at $r = R$ can be diagnosed in terms of v_{gr} and its radial derivative using the continuity equation (9.14).

The starting values for the temperature T_b and specific humidity q_b in the boundary layer are 25°C and 15 g kg^{-1}, respectively, giving a relative humidity of 72%.

[2]It is possible to take $C_{D0} + C_{D1}|\mathbf{u_b}(R)|$ and solve the equations for u_b and v_b numerically, but the result is essentially no difference from basing C_D on v_{gr}

The value for q_b is the same as the mixed layer value observed by Moss and Merceret (1976, Fig 4), but T_b cannot be compared with their observations as they showed only potential temperature.

With the starting values for u_b and v_b determined by Eqs. (2.45) and (2.46), Eqs. (2.37) - (2.39) may be solved numerically, given the radial profile v_{gr}. We choose $R = 500$ km. Radial profiles of selected dynamical quantities in the boundary layer and at the top of it are shown in Fig. 2.5 for this calculation. At large radii ($r > 350$ km), the mean vertical motion at the top of the boundary layer, $\overline{w}_\delta$, is downward and the total wind speed $|\mathbf{v_b}| = \sqrt{u_b^2 + v_b^2}$ is less than that at the top of the boundary layer, v_{gr}. As r decreases, both u_b and v_b increase in magnitude, as does v_{gr}, the maximum value of v_b occurring just inside the radius of maximum tangential wind speed (RMW) above the boundary layer. As a result, the frictional force, $\mathbf{F} = C_d|\mathbf{v_b}|\mathbf{v_b}/\delta$ increases, and in particular its radial component, F_r, denoted by fri in the top right panel of Fig 2.5. The net radially-inward pressure gradient force per unit mass, $(v_{gr}^2 - v_b^2)/r + f(v_{gr} - v_b)$, denoted by pgf, increases also with decreasing r, at least for large r, but more rapidly than the frictional force. The reason is that columns of fluid partially conserve their absolute angular momentum as they converge in the boundary layer and despite some frictional loss to the surface, their rotation rate increases. The increase in v_b is assisted by the downward transfer of tangential momentum from above, represented by the term $(w_{\delta-} + w_{sc})(v_b - v_{gr})/\delta$ in Eq. (2.38), although this effect turns out to be very small. The downward transfer of (zero) radial momentum, represented by the term $(w_{\delta-} + w_{sc})u_b/\delta$ in Eq. (2.37), is denoted by wu in Fig. 2.5, but this also makes a negligible contribution to the force balance in the boundary layer. For the typical tangential wind profile used, v_b increases faster than v_{gr} as r decreases inside a radius of about 200 km. In this region, pgf decreases faster than $wu + fri$ so that eventually the *net* radial force $pgf - wu - fri$ changes sign. This change occurs well before the RMW is reached. When $pgf - wu - fri$ becomes positive, the radial inflow decelerates, but v_b continues to increase as columns of air continue to move inwards. Eventually, v_b asymptotes to v_{gr} and pgf tends to zero, but at no point does the tangential wind speed become supergradient. Nevertheless, as pgf tends to zero, the net outward force, primarily due to friction, becomes relatively large and the inflow decelerates very rapidly. The mean vertical velocity at the top of the boundary layer increases steadily with decreasing r and reaches a maximum very close to the RMW: thereafter it decreases rapidly.

The lower right panel of Fig. 2.5 shows how the absolute angular momentum in the boundary layer decreases with decreasing radius as a result of the surface frictional torque. However, the rate of decrease is less rapid than that above the boundary layer and value in the boundary layer asymptotes to the value above the layer at inner radii.

It turns out that, except for a short adjustment length, which decreases in radial extent with increasing R, the calculations are relatively insensitive to the choice of R (see Smith, 2003). This insensitivity to R is not true of the thermodynamic fields

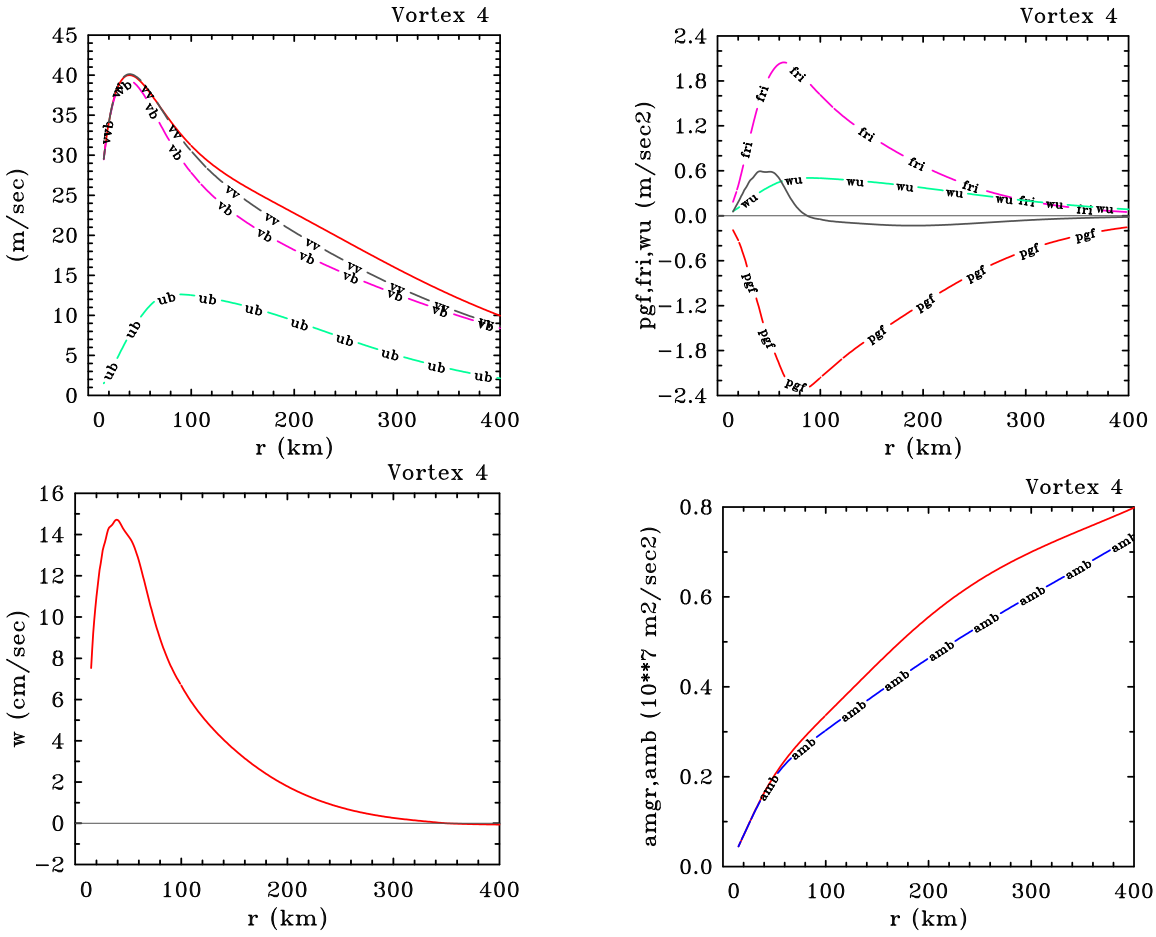

Figure 2.5: Radial profiles of selected dynamical quantities in the boundary layer calculation: (top left) tangential and radial components of wind speed in the boundary layer (u_b, v_b), total wind speed in the boundary layer, vv, and tangential wind speed above the boundary layer (v_{gr} - the unmarked solid line) [Units m s^{-1}]; (top, right) radial pressure gradient force (pgf) and frictional force (fri) per unit mass in the boundary layer, together with the force associated with the downward flux of radial momentum through the top of the boundary layer (wu) [Units 1.0×10^{-3} m s^{-2}] and the sum of these three forces (solid line); (bottom left) vertical velocity at the top of the boundary layer, w_δ [Units cm s^{-1}]; (bottom right) absolute angular momentum above the boundary layer (solid line) and in the boundary layer (amb) [Units 1.0×10^7 m^2 s^{-2}].

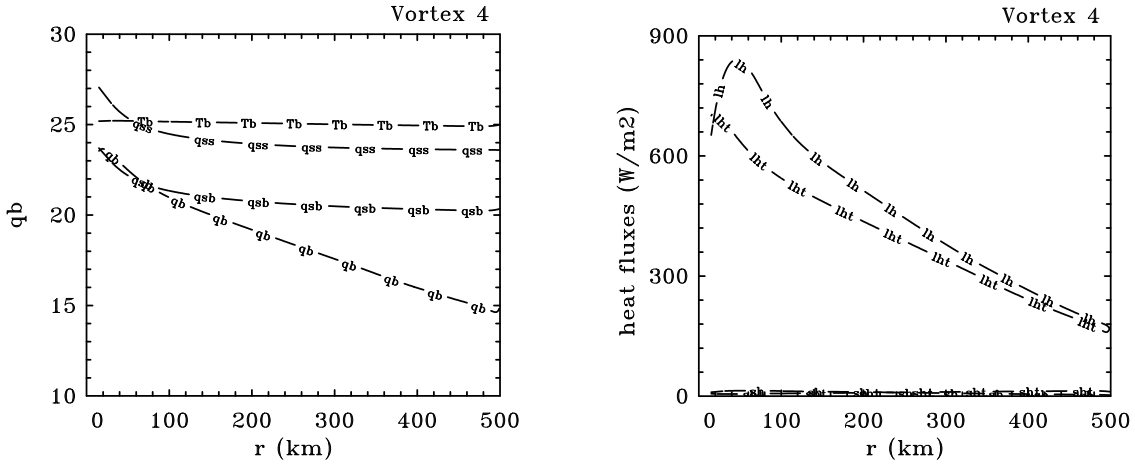

Figure 2.6: Radial profiles of selected thermodynamic quantities in the control calculation: (left panel) boundary layer temperature (Tb, unit deg. C), specific humidity (qb), saturation specific humidity (qsb), and the saturation specific humidity at the sea surface (qss) [Units gm kg^{-1}]; (right panel) latent heat fluxes from the sea surface (lh) and through the top of the boundary layer (lht)), and corresponding sensible heat fluxes (the two curves just above the abscissa labelled "sh" and "sht") [Units W m^{-2}].

as discussed below.

2.9.3 Thermodynamic aspects

The left panel of Fig. 2.6 shows the radial profiles of boundary layer temperature, specific humidity and saturation specific humidity, together with the saturation specific humidity at the sea surface temperature (q_{ss}), while the right panel shows the fluxes of sensible and latent heat at the surface and through the top of the boundary layer. At large radii, the wind speed is comparatively light and the boundary layer is in approximate[3] radiative-convective equilibrium. In particular, the air temperature just above the sea surface is only slightly lower than the sea surface temperature; the net sensible heat fluxes from the sea and through the top of the boundary layer approximately balance the radiative cooling; and the moistening of the boundary layer by the surface flux approximately balances the drying brought about by subsidence associated with shallow convection. The mass flux of shallow convection and the boundary layer depth are chosen to ensure this balance.

As r decreases and the surface wind speed increases, the surface moisture flux increases and the boundary layer progressively moistens. The increase in moisture contrast between the boundary layer and the air aloft leads to an increase in the flux

[3]The radiative-convective state is very sensitive to the choice of parameters including the mass flux of shallow convection and the boundary layer depth. We choose rounded numbers for these quantities so that the boundary layer is close to, but not exactly in equilibrium.

of dry air through the top of the subcloud layer, which reduces the rate of moistening. This effect would be reduced in a more complete model in which the moisture content above the boundary layer is predicted. If shallow convection and radiative cooling are omitted, the rate of moistening is relatively rapid and the boundary layer saturates (i.e. $q_b = q_s$ at a relatively large radius (453 km), although, of course, then the boundary layer is not in radiative-convective equilibrium at $r = R$. In the present case, saturation occurs at a radius of about 80 km, but the air just above the sea surface does not (i.e. $q_b < q_{ss}$), which in terms of the simple model could be interpreted to mean that the boundary layer becomes topped by low cloud. A further consequence is that the surface moisture fluxes do not shut off. We have not allowed for the latent heat release in the inner core in these calculations as the degree of supersaturation is only about 1% (see Smith, 2003, Fig. 11). The degree of moisture disequilibrium at the sea surface is maintained by the fact that the saturation specific humidity increases as the surface pressure decreases. The latent heat fluxes are much larger than the sensible heat fluxes.

2.10 Radiative cooling

The tropical atmosphere is stably stratified so that large vertical displacements of air parcels may only occur in the presence of diabatic processes: parcel ascent can occur over significant depths only if there is latent heat release to counter adiabatic cooling (i.e. if the ascent occurs in cloud); and parcel subsidence can occur over a substantial depth only if there is radiative cooling to counter adiabatic warming. Thus radiative effects in tropical cyclones cannot be ignored if we wish to understand the subsiding branch of the secondary circulation. The following discussion of radiative effects is based on that of Anthes (1979, p218-9).

Diabatic heating rates associated with the absorption of shortwave radiation energy and the emission of longwave radiation are quite small compared with the heating rates associated with condensation in deep precipitating clouds. In the cloud-free regions of the tropical atmosphere the mean radiative cooling rate is 1 to 2°C/day from the surface to 10 km ($\approx$ 250 mb) and decreases to about zero at the tropopause. In a region of multi-layer clouds, however, there is practically no radiative cooling in the clouds, but there is strong cooling at their top.

The result of differential radiative heating between the cloud-free environment and a cloudy tropical depression or tropical cyclone is to generate a direct circulation, with sinking motion in the clear air and rising motion in the cloudy air (Fig. 2.7). In the tropical cyclone, radiation acts to maintain the baroclinicity associated with the warm core. However, it is a smaller effect than differential heating by condensation, except possibly in lightly precipitating systems. This may be seen by relating the mean diabatic rate of temperature in a column of air of unit cross-section extending from 1000 mb to 100 mb to the rainfall rate R_f (cm/day):

$$\frac{\partial T}{\partial t} = -2.67 R_f \quad (^o\text{C/day}). \tag{2.47}$$

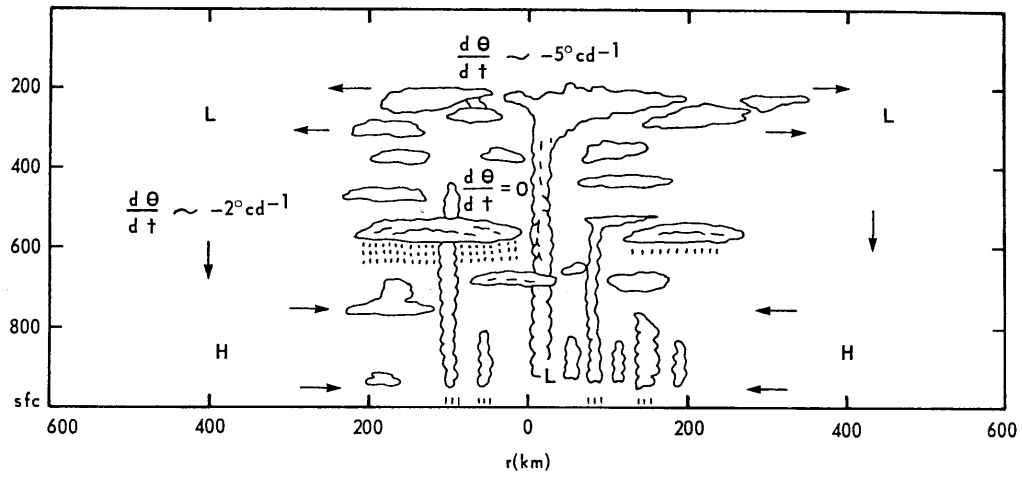

Figure 2.7: Schematic diagram of radiatively-induced circulation in a tropical disturbance. In clear air surrounding the cloudy centre, diabatic cooling is about 2°C/day. In the cloudy interior, radiative cooling is nearly zero. The differential cooling induces sinking motion in the environment, where pressures rise at the surface and fall aloft. Flow in low levels is toward the centre of the disturbance, aloft it is outward. (From Anthes, 1979)

For typical cloud cluster rainfall rates of 2.5 cm/day (Ruprecht and Gray, 1976), the average tropospheric rate of temperature change would be 6.7 cm/day, which is about five times larger than the effect of radiation. For hurricanes, a typical rainfall rate in the inner 222 km region is 9.5 cm/day, which gives $\partial T/\partial t = -25°$C/day, more than an order of magnitude larger than the radiative cooling rate. Thus, without latent heat release, only a slow meridional circulation could be maintained by radiation because the lifting of statically-stable air leads to cooling and a negative buoyancy force that opposes the circulation induced by radiative cooling. With latent heating, however, the mean adiabatic cooling in the ascending branch of the secondary circulation is opposed and much larger upward velocities may be attained.

When direct absorption of shortwave solar radiation is considered, a diurnal variation of the radial differential cooling rate is introduced. The differential cooling during the day is reduced from a nocturnal value of 2°C/day to a value of about 1°C/day in the middle troposphere. For $\partial T/\partial p \approx 8°$C/(100 mb), $\partial T/\partial t \approx 1°$C/day corresponds to a vertical velocity ω of about 12.5 mb/day, which is supported by a mean divergence of 5×10^{-7} s^{-1} between the surface and 500 mb. This is much smaller than the observed diurnal variation in low-level divergence, which is about 5×10^{-6} s^{-1} (Gray and Jacobson, 1977). What probably happens is that the small diurnal variation in radiation-induced divergence triggers a much larger response by modulating deep cumulus convection. During the night, when differential cooling is at a maximum, upper-level divergence over the disturbance and low-level conver-

gence into the disturbance results in a dramatic increase in convection. After sunrise, absorption of solar radiation in the cloud-free environment and increased subsidence from the enhanced secondary circulation during the night reduces the mean temperature difference between the disturbance and its environment. The mean circulation then diminishes and the deep cumulus clouds weaken.

2.11 The Emanuel steady-state model

The basis of Emanuel's steady-state model for a tropical cyclone, described by Emanuel (1986), is Fig. 2.4. It is convenient to divide the domain into three regions as shown in Fig. 2.8. Regions I and II encompass the eye and eyewall regions, respectively, while Region III refers to that beyond the eyewall clouds. Region II is where the upward mass flux at the top of the boundary layer is large compared with that associated with shallow convection. Smith (2003, p1013) estimated a value for w_{sc} (defined in section 2.9.1) of about 2 cm s^{-1}, based on the radiative equilibrium of the boundary layer at some large radius. In the boundary layer calculation shown in Fig. 2.5, $w > 5w_{sc}$ for $r < 2r_m$, where r_m is the radius of maximum tangential wind speed above the boundary layer. By comparison, Emanuel *op. cit.* takes the outer radius of Region II to be r_m.

In pressure coordinates, the gradient wind equation and hydrostatic equation may be written as:

$$g\left(\frac{\partial z}{\partial r}\right)_p = \frac{M^2}{r^3} - \tfrac{1}{4} r f^2 \tag{2.48}$$

and

$$g\left(\frac{\partial z}{\partial p}\right)_r = -\alpha, \tag{2.49}$$

where $\alpha = 1/\rho$ is the specific volume. Eliminating the geopotential height of the pressure surface, gz, gives an alternative form of the thermal wind equation:

$$\frac{1}{r^3}\left(\frac{\partial M^2}{\partial p}\right)_r = -\left(\frac{\partial \alpha}{\partial r}\right)_p. \tag{2.50}$$

At this point it is convenient to introduce the saturation moist entropy, s^*, defined by:

$$s^* = \ln \theta_e{}^*, \tag{2.51}$$

which is a state variable. Therefore we can regard α as a function of p and s^* and with a little manipulation we can express the thermal wind equation as:

$$\frac{1}{r^3}\left(\frac{\partial M^2}{\partial p}\right)_r = -\left(\frac{\partial \alpha}{\partial s*}\right)_p \left(\frac{\partial s^*}{\partial r}\right)_p. \tag{2.52}$$

I will show in an Appendix 2.16.1 that

$$\left(\frac{\partial \alpha}{\partial s^*}\right)_p = \left(\frac{\partial T}{\partial p}\right)_{s*}, \tag{2.53}$$

whereupon Eq. (2.52) becomes

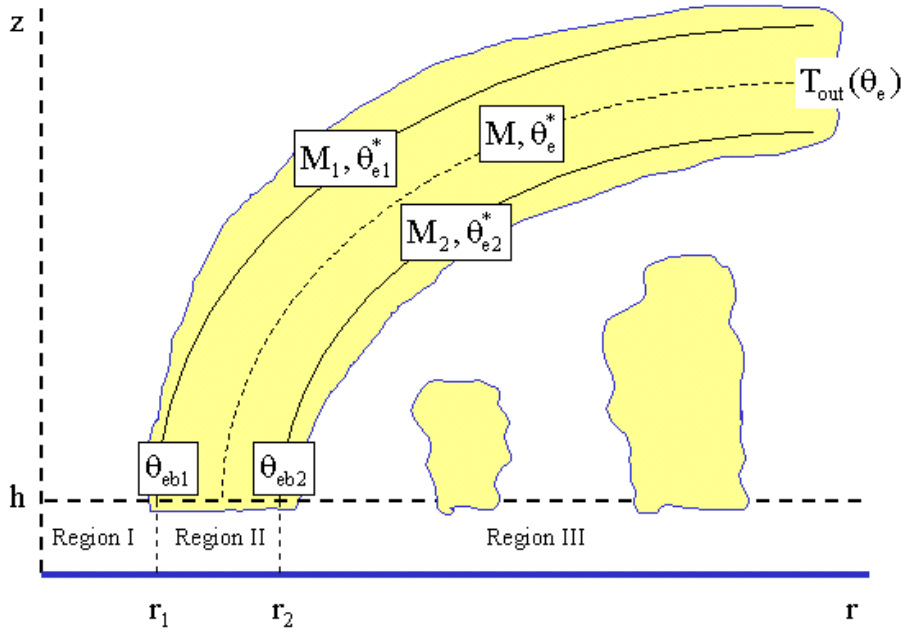

Figure 2.8: Schematic diagram of the secondary circulation of a mature tropical cyclone showing the eye and the eyewall clouds. The absolute angular momentum per unit mass, M, and equivalent potential temperature, θ_e of an air parcel are conserved after the parcel leaves the boundary layer and ascends in the eyewall clouds. The precise values of these quantities depend on the radius at which the parcel exits the boundary layer. At radii beyond the eyewall cloud, shallow convection plays an important role in moistening and cooling the lower troposphere above the boundary layer and warming and drying the boundary layer as indicated.

$$\frac{1}{r^3}\left(\frac{\partial M^2}{\partial p}\right)_r = -\left(\frac{\partial T}{\partial p}\right)_{s*}\left(\frac{\partial s^*}{\partial r}\right)_p . \tag{2.54}$$

With the assumption that M and s^* surfaces coincide, i.e. $M = M(s^*)$, Eq. (2.54) becomes

$$\frac{2M}{r^3}\left(\frac{\partial M}{\partial p}\right)_r = -\left(\frac{\partial T}{\partial p}\right)_{s*}\frac{ds^*}{dM}\left(\frac{\partial M}{\partial r}\right)_p . \tag{2.55}$$

Note that $\partial T/\partial p)_{s*}$ is just the temperature lapse rate as a function of pressure along a moist adiabat. Now along an M surface,

$$\left(\frac{\partial M}{\partial r}\right)_z \delta r + \left(\frac{\partial M}{\partial p}\right)_r \delta p = 0, \tag{2.56}$$

so that the slope of an M surface in (r, p) space is

$$\left(\frac{dr}{dp}\right) = -\left(\frac{\partial M}{\partial p}\right)_r / \left(\frac{\partial M}{\partial r}\right)_p. \tag{2.57}$$

Using Eq. (2.57) this equation gives

$$\frac{1}{2}\left(\frac{dr^{-2}}{dp}\right)_M = -\frac{1}{2M}\left(\frac{\partial T}{\partial p}\right)_{s*}\frac{ds^*}{dM}, \tag{2.58}$$

which may be integrated upwards along the M (or s^*) surface to give

$$\frac{1}{r^2}|_M - \frac{1}{r_{out}^2}|_M = \frac{1}{M}\frac{ds^*}{dM}[T - T_{out}(s^*, p_{out})], \tag{2.59}$$

where T_{out} is the outflow temperature along the M (or s^*) surface at some large radius r_{out}. If we assume that the air in the boundary layer and, in particular at the top of this layer $z = h$, is a constant[4], T_B, and that $r << r_{out}$, then

$$-r^2\frac{ds^*}{dM}[T_B - T_{out}(s^*, p_{out})] = M, \text{ at } z = h, \tag{2.60}$$

or, alternatively,

$$-[T_B - T_{out}(s^*, p_{out})]\frac{\partial s^*}{\partial r} = \frac{1}{2r^2}\frac{\partial M^2}{\partial r}, \text{ at } z = h. \tag{2.61}$$

At this stage it is convenient to use the Exner function, π, instead of pressure. Then the gradient wind equation takes the form

$$M^2 = r^3\left[c_p T_B\frac{\partial \ln \pi}{\partial r} + \frac{1}{4}rf^2\right], \tag{2.62}$$

whereupon Eq. (2.61) can be written

$$-\frac{T_B - T_{out}(s^*, p_{out})}{T_B}\frac{\partial \ln \theta_e}{\partial r} = \frac{\partial \ln \pi}{\partial r} + \frac{1}{2}\frac{\partial}{\partial r}\left(r\frac{\partial \ln \pi}{\partial r}\right) + \frac{1}{2}\frac{rf^2}{c_p T_B}, \text{ at } z = h, \tag{2.63}$$

where it is assumed that $\theta_e^* = \theta_e$ at the top of the boundary layer.

Equation 2.63 may be integrated with respect to radius from r to some value r_o giving

$$\begin{aligned} &-\ln \theta_{eo} + \ln \theta_e + \frac{1}{T_B}\int_r^{r_o} T_{out}(s^*, p_{out})\frac{\partial \ln \theta_e}{\partial r}dr \\ &= \ln \pi_o - \ln \pi + \frac{1}{2}\left(r\frac{\partial \ln \pi}{\partial r}\right)_o - \frac{1}{2}\left(r\frac{\partial \ln \pi}{\partial r}\right) + \frac{1}{4}\frac{f^2}{c_p T_B}(r_o^2 - r^2), \text{ at } z = h. \end{aligned} \tag{2.64}$$

[4]According to the boundary layer model described in section 2.9, this is not a bad assumption if the sea surface temperature is uniform.

We define

$$\bar{T}_{out} = \frac{1}{\ln(\theta_e^*/\theta_{eo})} \int_{\ln\theta_{eo}}^{\ln\theta_e^*} T_{out} d\ln\theta_e^*, \tag{2.65}$$

which is average outflow temperature weighted with the saturation moist entropy of the outflow angular momentum surfaces. Remember that θ_e^* along angular momentum surfaces is taken equal to θ_e where the surfaces meet the top of the boundary layer. Then (2.61) gives

$$\frac{T_B - \bar{T}_{out}}{T_B} \ln\left(\frac{\theta_e}{\theta_{eo}}\right) = \ln(\pi_o/\pi) + \frac{1}{2}\left(r\frac{\partial \ln\pi}{\partial r}\right)_{r_o} - \frac{1}{2}\left(r\frac{\partial \ln\pi}{\partial r}\right)$$

$$+\frac{1}{4}\frac{f^2}{c_p T_B}(r_o^2 - r^2) \text{ at } z = h. \tag{2.66}$$

This relationship between the radial pressure distributions $p(r)$ and θ_e, valid in Region II, exerts a powerful constraint on the structure of the mature steady axisymmetric tropical cyclone and is at the heart of the steady-state hurricane model developed by Emanuel (1986).

To complete the model in this region it is necessary to consider the dynamics and thermodynamics of the boundary layer. The plan will be to derive a second relationship between $p(r)$ and θ_e. The boundary layer imposes a further constraint on the steady solution as it determines the radial distribution of both M and θ_e where the flow exits the layer. Referring to the previous section, it is possible to define a streamfunction ψ for the flow in the boundary layer, given by:

$$\rho r u_b = -\frac{\partial\psi}{\partial z}, \quad \rho r w_b = \frac{\partial\psi}{\partial r} \tag{2.67}$$

Then

$$u_b = -\frac{\psi(r,h)}{\rho r h}, \quad w_b = \frac{1}{\rho r}\frac{\partial\psi}{\partial r} \tag{2.68}$$

Let φ_b be the absolute angular momentum M or the moist entropy, s. Then φ_b satisfies

$$\psi(r,h)\frac{d\varphi_b}{dr} - r w_h[\varphi_h - \varphi_b] = -\frac{r}{\rho}\tau_\varphi(r,0) \tag{2.69}$$

where τ_φ is the surface flux of φ. If the flow is out of the boundary layer, $(w > 0)$, then $\varphi_h = \varphi_b$ and neglecting shallow convection (see subsection 2.8.1), φ_b satisfies

$$\psi(r,h)\frac{d\varphi_b}{dr} = -\frac{r}{\rho}\tau_\varphi(r,0) \tag{2.70}$$

whereas if it is into the boundary layer $(w < 0)$,

$$\psi(r,h)\frac{d\varphi_b}{dr} = -\frac{r}{\rho}\tau_\varphi(r,0) + r w_h[\varphi_h - \varphi_b] \tag{2.71}$$

Then in Region II in Fig. 2.8, where the flow is out of the boundary layer,

$$\left.\frac{\partial s}{\partial M}\right|_{z=h} = \left.\frac{\tau_s}{\tau_M}\right|_{z=h} \tag{2.72}$$

The standard aerodynamic formulae are used for surface fluxes:

$$\begin{aligned} \tau_s &= -c_p C_k |\mathbf{V}|(\ln\theta_e - \ln\theta_{es}) \\ \tau_M &= -C_D |\mathbf{V}| r V, \end{aligned} \tag{2.73}$$

where $|\mathbf{V}|$ is the magnitude of the surface horizontal velocity, C_k and C_D are exchange coefficients for enthalpy and momentum and θ_{es} is the saturation equivalent potential temperature at the sea surface temperature.

$$\ln\theta_e = \ln\theta_{es} - \frac{C_D}{C_k}\frac{1}{c_p(T_B - \bar{T}_{out})}\left(V^2 + \frac{1}{2}rfV\right), \text{ at } z = h, \tag{2.74}$$

where Eq. (2.9) has been used to express M in terms of V. Note that C_D and C_k do not enter separately, but only as a ratio. Since $V(r)$ is related to $p(r)$, Eq. (2.74) provides an additional constraint relating θ_e and $p(r)$. The other constraint is Eq. (2.66).

In Region II, $rf << V$ so that the gradient wind equation may be written

$$V^2 \approx c_p T_B r \frac{\partial \pi}{\partial r}. \tag{2.75}$$

Then θ_e may be eliminated between Eqs. (2.74) and (2.65) to yield an equation for pressure alone, which, in turn, through the gradient wind equation, determines the velocity profile at the top of the boundary layer.

In Region III we must use Eq. (2.71) rather than Eq. (2.70), but we do not have an expression for w_h. Emanuel (1986) circumvented this problem and assumed that the combined effect of boundary-layer-induced subsidence and turbulent fluxes at the top of the boundary layer is to bring the relative humidity of the boundary layer to a relatively uniform level of 80%. This allows one to obtain a second relationship between θ_e and $p(r)$ in Region III also. The derivation starts from the approximate formula for θ_e:

$$\ln\theta_e = \ln T - \ln\pi + \frac{Lq}{c_p T}. \tag{2.76}$$

With the assumption that T does not vary with radius ($= T_B$), and that θ_e is uniform through the depth of the boundary layer we obtain:

$$\ln\theta_e - \ln\theta_{ea} = -\ln\pi + \ln\pi_a + \frac{L}{c_p T_B}(q - q_a) \text{ at } z = h, \tag{2.77}$$

where a suffix "a" refers to ambient values. Now the hydrostatic equation may be written as $d\ln\pi/dz = g/(c_p T)$, whereupon

$$\ln\pi_{(z=h)} = \ln\pi_{(z=0)} + \int_0^h \frac{g dz}{c_p T},$$

and if T does not vary with radius, $\ln(\pi_s/\pi_h) = \ln(\pi_{sa}/\pi_{ha})$, where the suffix "s" refers to surface values. Then Eq. (2.77) becomes

$$\ln \frac{\theta_e}{\theta_{ea}} = -\ln \frac{\pi_s}{\pi_{sa}} + \frac{L}{c_p T_B}(q_s^* RH - q_{sa}^* RH_a). \tag{2.78}$$

Now $q \approx \epsilon e^*(T_B)/p$, whereupon $q^* = {q_a}^*(p_{sa}/p_s) = {q_a}^*(\pi_{sa}/\pi_s)^{1/\kappa} = \exp[(1/\kappa)(\pi_{sa}/\pi_s)]$. Then if $RH = RH_a$,

$$\ln \frac{\theta_e}{\theta_{ea}} = -\ln \frac{\pi_s}{\pi_{sa}} \left[1 + \frac{L{q_{as}}^* RH_a}{RT_B}\right]. \tag{2.79}$$

This is the desired second relationship between θ_e and $p(r)$ in Region III, but note that it is obtained from thermodynamic considerations alone.

Emanuel *op. cit.* presents an analysis in an appendix to show that with the assumption that the eye is in solid body rotation, the M-surfaces and s^* surfaces approximately coincide and he uses this result to apply the relation (2.66) in Region I also. Moreover he assumes that (2.74) applies also in the boundary layer within the eye. Then the radial variation of surface pressure can be obtained by solving the last two relationships in Regions I and II and Eqs. (2.66) and (2.79) in Region III and matching these solutions at the boundary between Regions II and III, which, as noted earlier, Emanuel takes to be at radius r_m. Then the gradient wind equation may be used to find the tangential wind speed at the top of the boundary layer. Finally the solution for the flow above the boundary layer may be obtained by evaluating quantities along angular momentum surfaces, whose shape is given by (2.59), which may be written as

$$\frac{1}{r^2}|_M = \frac{1}{M}\frac{ds^*}{dM}[T - T_{out}(s^*, p_{out})],$$

on the assumption that $r << r_{out}$. The reader is referred to Emanuel's paper for details of the calculations. Emanuel shows an example of a calculation for the following parameter values: $T_s = 27^o$C, $T_B = 22^o$C, $T_{out} = -67^o$C, f evaluated at 28^o latitude, $p_o = 1015$ mb, $r_o = 400$ km, $C_\theta = C_D$, $RH_a = 80\%$, and $\gamma = 2$, corresponding to a Brunt-Väsälä frequency of 1.5×10^{-2}. Under these conditions the central pressure is 941 mb, the maximum tangential wind speed is 58 m s^{-1}, the radius of maximum winds is 36 km, and the ambient boundary layer θ_e is 349 K. The distributions of M, θ_e^*, V, and the temperature perturbation from the far environment at the same altitude are shown in Fig. 2.9. The solution captures the main observed features of a mature hurricane including the warm core at high altitude, the outward-sloping velocity maximum, and the strong radial gradient of θ_e^* near and inside the radius of maximum tangential wind speed.

Emanuel *op. cit.* estimated the streamfunction at the top of the boundary layer assuming that Eq. (2.70) gives the correct momentum balance in the boundary layer without considering turbulent fluxes at the top of the layer, even if the neglect of such fluxes yields an incorrect heat budget. Setting $\varphi_b = M$ in (2.70) and using (2.70) we can solve for the boundary-layer streamfunction, from which we can obtain the

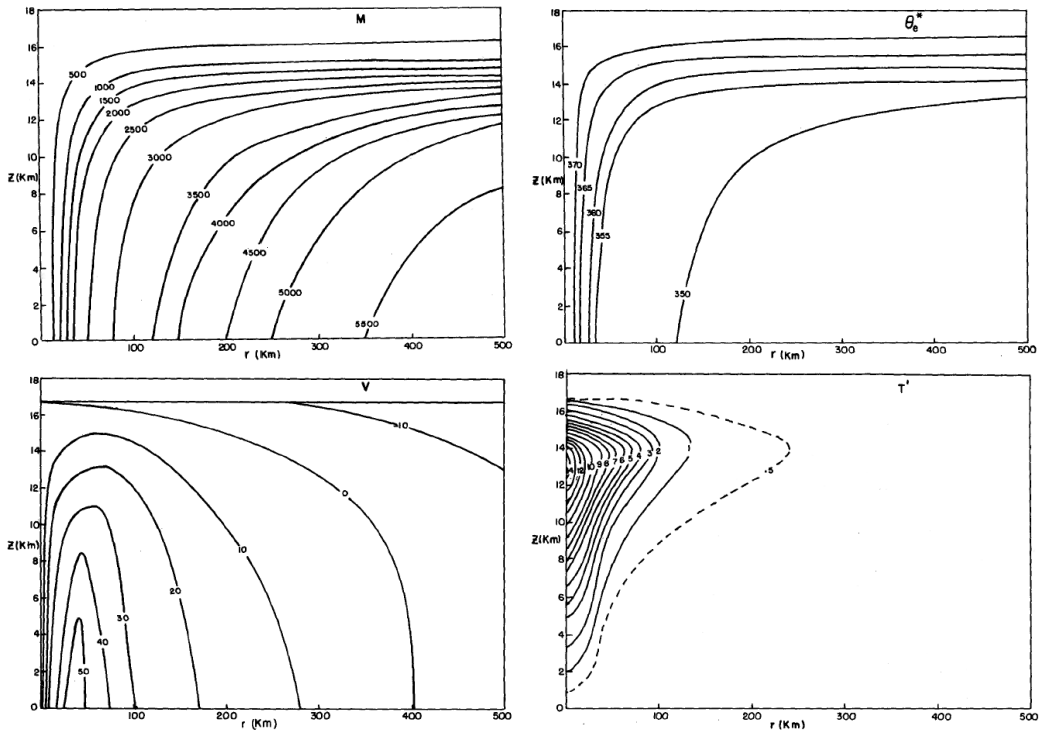

Figure 2.9: Distributions of: (a) absolute angular momentum (10^3 m^2 s^{-1}), (b) saturation equivalent potential temperature, (c) gradient wind (m s^{-1}), and (d) temperature departure (^{o}C) from the far environment at the same altitude, for the vortex discussed above. (From Emanuel 1986)

vertical velocity using $\rho r w_h = \partial\psi/\partial r$. The mean radial velocity in the boundary layer is given by $r\bar{u} = -\psi/(\bar{\rho}h)$, where h is the nominal depth of the layer and $\bar{\rho}$ is the mean density. The radial distributions of w_h and $\bar{u}$ for the vortex described above are shown in Fig. 2.10. These calculations are based on the assumptions that $\bar{\rho}$ and h are constants, with $h = 1$ km, and $C_D = 2 \times 10^{-3}$.

The vertical velocity profile in Fig. 2.10 shows a sharp peak at the radius of maximum tangential wind, but radial velocity reaches its maximum at a much larger radius. This is similar to the behaviour in the boundary-layer calculation shown in Fig. 2.5. Here, however, the streamfunction has a discontinuity at r_{max} as a consequence of matching two separate boundary layers there, since the radial gradient of angular momentum is discontinuous. This results in a jump in u and a delta function spike of vertical velocity at r_{max}. According to Emanuel, these unrealistic features would not be present had a single boundary layer representation been applied throughout the vortex. Note that w_h becomes negative beyond a radius of about 220 km, which is not consistent with the choice of r_o as 400 km.

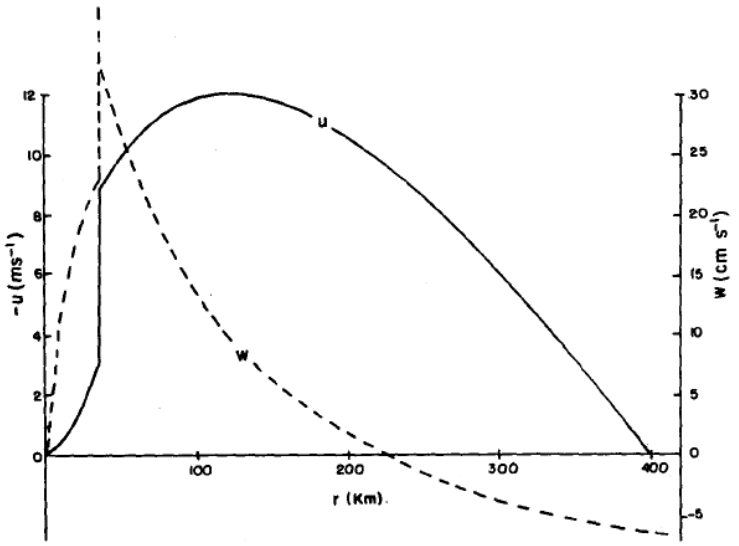

Figure 2.10: Radial distributions of vertical velocity (cm s^{-1}), and mean radial velocity (m s^{-1}) within the boundary layer for the vortex discussed above. (From Emanuel 1986)

2.12 The tropical cyclone as a Carnot heat engine

Emanuel suggests that the steady tropical cyclone may be regarded as a simple Carnot heat engine in which air flowing inwards in the boundary layer acquires moist entropy from the sea surface, ascends, and ultimately gives off heat at the much lower temperature of the upper troposphere or lower stratosphere. A schematic of this heat engine is shown in Fig. 2.11. Air begins to flow inwards at constant temperature along the lower boundary at radius r_o and acquires an incremental amount of heat

$$\Delta Q_1 = \int_{\theta_{ea}}^{\theta_e} c_p T_B d\ln\theta_e = c_p T_B \ln\left(\frac{\theta_e}{\theta_{ea}}\right), \tag{2.80}$$

where θ_{ea} is the equivalent potential temperature at r_o. The air ascends at constant entropy along an M surface and flows out to large radius. To complete the circuit, the air eventually loses enough total heat through radiative cooling to return to its ambient θ_e so that

$$\Delta Q_2 = \int_{\theta_e}^{\theta_{ea}} c_p T_{out} d\ln\theta_e = -c_p T_{out} \ln\left(\frac{\theta_e}{\theta_{ea}}\right), \tag{2.81}$$

where T_out is given by (19). The total heating, from (57) and (58), is therefore

$$\Delta Q = \Delta Q_1 + \Delta Q_2 = c_p T_B \epsilon \ln\left(\frac{\theta_e}{\theta_{ea}}\right), \tag{2.82}$$

where $\varepsilon = (T_B - T_{out})/T_B$ is the thermodynamic efficiency. This net heating is used to do work against frictional dissipation in the steady tropical cyclone. Referring to Fig. 2.11, it is seen that work is done against friction in the inflowing boundary-layer air and also to change the angular momentum back to its ambient value at large radii in the outflow. Kinetic energy is also dissipated by turbulence within cumulus clouds; however, Emanuel argues that this sink primarily balances kinetic energy generated by release of the ambient convective available potential energy as is probably the case in the unperturbed tropical atmosphere. This is simply a statement that convective clouds in tropical cyclones are locally similar to those away from such disturbances. The balance between total heating and frictional dissipation in the inflow and outflow may be written symbolically as

$$\Delta Q = W_{PBL} + W_o, \tag{2.83}$$

where W_{PBL}, and W_o are the work done in the boundary layer and outflow, respectively. The latter is simply proportional to the change in kinetic energy needed to bring the angular momentum of the outflow, M, back to its ambient value M_o:

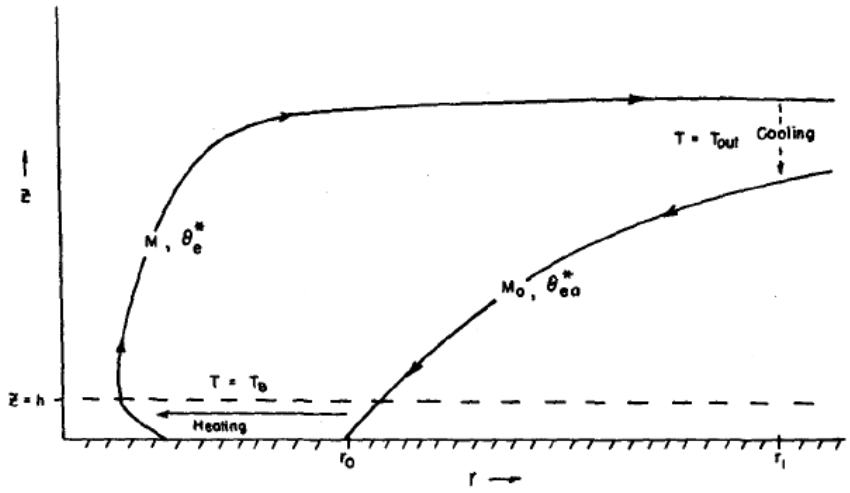

Figure 2.11: The tropical cyclone as a Carnot heat engine.

$$\begin{aligned} W_0 &= \frac{1}{2}\Delta V^2 = \frac{1}{2}\left[\left(\frac{M}{r_1} - \frac{1}{2}fr_1\right)^2 - \left(\frac{M_0}{r_1} - \frac{1}{2}fr_1\right)^2\right] \\ &= \frac{1}{2}\left[\frac{M^2 - M_0^2}{r_1^2} + f\left(M_0 - M\right)\right], \end{aligned} \tag{2.84}$$

where we have related azimuthal velocity to angular momentum using (1) and r_1 is some large radius at which the exchange takes place. In the limit of large r_1,

$$\lim_{r_1 \to 0} W_0 = \frac{1}{2}f(M_0 - M) = \frac{1}{4}f^2(r_0^2 - r^2) - \frac{1}{2}frV. \tag{2.85}$$

Using the above (2.82) and (2.83) we infer the work done in the boundary layer:

$$W_{PBL} = C_P T_B \varepsilon \ln \frac{\theta_e}{\theta_{ea}} + \frac{1}{2} frV - \frac{1}{4} f^2 \left(r_0^2 - r^2 \right). \tag{2.86}$$

Finally, knowledge of the work done against dissipation in the boundary layer allows an evaluation of the pressure distribution in the boundary layer through the use of Bernoulli's equation. The latter, when integrated inward from r_0 at constant temperature, may be written

$$\frac{1}{2} V^2 + C_P T_B \varepsilon \ln \pi + W_{PBL} = 0 \quad \text{at} \quad z = 0. \tag{2.87}$$

When (2.86) is substituted into this and the gradient wind equation is used for the sum $V^2 + frV$, the result is

$$\ln \pi + \frac{1}{2} r \frac{\partial \ln \pi}{\partial r} + \varepsilon \ln \frac{\theta_e}{\theta_{ea}} - \frac{1}{4} \frac{f^2}{C_p T_B} (r_0^2 - r^2) = 0 \quad \text{at} \quad z = 0, \tag{2.88}$$

which is identical to (2.66). This confirms the interpretation of the results of the previous section in terms of a Carnot engine.

2.13 Tropical cyclone intensity change

We have seen in section 2.3 that if there is no friction and no diabatic forcing ($\dot{\theta} = 0$), Eqs. (2.1) - (2.6) admit steady axisymmetric solutions of the form $(0, v(r, z), 0)$ in cylindrical coordinates. Axisymmetric vortices intensify as a result of radial inflow above the boundary layer on account of the conservation of angular momentum. We have seen in section 2.4 that the presence of surface friction induces radial inflow in the boundary layer and ascent or descent at the top of the boundary layer. If there is no diabatic forcing there must be radial outflow above the boundary layer otherwise friction alone would lead to intensification of the primary vortex. Because the air above the boundary layer is stably-stratified, the outflow tends to occur in a layer of limited depth above the boundary layer. It is clear that intensification requires a mechanism to produce inflow that is strong enough to oppose the outflow induced by surface friction. The only conceivable mechanism able to do this is diabatic heating arising from the latent heat release in deep clouds, which produces *buoyancy* in the clouds. We consider here a balanced axisymmetric theory for intensity change, i.e. one in which the flow remains close to hydrostatic and gradient wind balance. In a later chapter we consider idealized numerical modelling studies of tropical-cyclone intensification. As a preliminary step we examine the definition of buoyancy and its generalization for a rapidly-rotating fluid. Later we will examine other aspects of the buoyancy force.

2.14 The secondary circulation

If the vortex is axisymmetric and in approximate geostrophic and hydrostatic balance, we can derive an equation for the streamfunction, ψ, of the circulation in a vertical plane, the so-called secondary circulation. This streamfunction is such that

$$u = -\frac{1}{r\rho}\frac{\partial \psi}{\partial z} \qquad w = \frac{1}{r\rho}\frac{\partial \psi}{\partial r}. \tag{2.89}$$

which ensures that the continuity equation (2.4), is satisfied. The equation for ψ follows by differentiating the thermal wind equation in the form (2.19) with respect to time t and using the azimuthal momentum equation and thermodynamic equation to eliminate the time derivatives. It is convenient to write the last two equations in the form

$$\frac{\partial v}{\partial t} + u(\zeta + f) + wS = \dot{V} \tag{2.90}$$

and

$$\frac{\partial \chi}{\partial t} + u\frac{\partial \chi}{\partial r} + w\frac{\partial \chi}{\partial z} = -\chi^2\dot{\theta} \tag{2.91}$$

where $\zeta = (1/r)(\partial(rv)/\partial r)$ is the relative vorticity and we have added a momentum source term $\dot{V}$ in the former equation for reasons that will emerge later. The time derivative of (2.14) is

$$g\frac{\partial}{\partial r}\frac{\partial \chi}{\partial t} + \frac{\partial}{\partial z}\left(C\frac{\partial \chi}{\partial t} + \chi\frac{\partial C}{\partial t}\right) = 0$$

and substitution of the time derivatives from (2.90) and (2.91) gives

$$g\frac{\partial}{\partial r}\left(u\frac{\partial \chi}{\partial r} + w\frac{\partial \chi}{\partial z} - Q\right) + \frac{\partial}{\partial z}\left[C\left(u\frac{\partial \chi}{\partial r} + w\frac{\partial \chi}{\partial z} - Q\right) + \chi\xi\left(u(\zeta + f) + wS - \dot{V}\right)\right] = 0$$

where $\chi = 1/\theta$ and $Q = -\chi^2\dot{\theta}$. Then

$$\frac{\partial}{\partial r}\left[g\frac{\partial \chi}{\partial z}w + g\frac{\partial \chi}{\partial r}u\right] +$$

$$\frac{\partial}{\partial z}\left[(\chi\xi(\zeta + f) + C\frac{\partial \chi}{\partial r})u + \frac{\partial}{\partial z}(\chi C)w\right] = g\frac{\partial Q}{\partial r} + \frac{\partial}{\partial z}(CQ) + \frac{\partial}{\partial z}(\chi\xi\dot{V})$$

or

$$\frac{\partial}{\partial r}\left[g\frac{\partial \chi}{\partial z}w - \frac{\partial}{\partial z}(\chi C)u\right] +$$

$$\frac{\partial}{\partial z}\left[(\chi\xi(\zeta + f) + C\frac{\partial \chi}{\partial r})u + \frac{\partial}{\partial z}(\chi C)w\right] = g\frac{\partial Q}{\partial r} + \frac{\partial}{\partial z}(CQ) + \frac{\partial}{\partial z}(\chi\xi\dot{V}) \tag{2.92}$$

using (2.19). Then substitution for u and w from Eqs. (2.89) into Eq. (2.92) gives

$$\frac{\partial}{\partial r}\left[g\frac{\partial\chi}{\partial z}\frac{1}{\rho r}\frac{\partial\psi}{\partial r}+\frac{\partial}{\partial z}(\chi C)\frac{1}{\rho r}\frac{\partial\psi}{\partial z}\right]-$$

$$\frac{\partial}{\partial z}\left[\left(\xi\chi(\zeta+f)+C\frac{\partial\chi}{\partial r}\right)\frac{1}{\rho r}\frac{\partial\psi}{\partial z}-\frac{\partial}{\partial z}(\chi C)\frac{1}{\rho r}\frac{\partial\psi}{\partial r}\right]=g\frac{\partial Q}{\partial r}+\frac{\partial}{\partial z}(CQ)+\frac{\partial}{\partial z}(\chi\xi\dot{V}) \tag{2.93}$$

This is called the *Sawyer-Eliassen equation* following the work of Eliassen (1951) and Sawyer (1956) (Sawyer derived a similar equation for frontal circulations in rectangular geometry). The equation was investigated in context of the tropical cyclones by Willoughby (1979) and Shapiro and Willoughby (1982). The discriminant of the Sawyer-Eliassen equation is

$$D=-g\frac{\partial\chi}{\partial z}\left(\xi\chi(\zeta+f)\partial z+C\frac{\partial\chi}{\partial r}\right)-\left[\frac{\partial}{\partial z}(\chi C)\right]^2 \tag{2.94}$$

Comparison with Eq. (5) of Shapiro and Willoughby (1982) shows that Eq. (2.93) is elliptic if $D>0$.

The Sawyer-Eliassen equation contains three spatially-varying parameters characterizing:

- the *static stability*
$$N^2=-g\frac{\partial\chi}{\partial z};$$
- the *inertial stability*
$$I^2=-\frac{1}{r^3}\frac{\partial M^2}{\partial r}=\xi\zeta;$$
- the *baroclinicity*
$$B^2=-\frac{1}{r^3}\frac{\partial M^2}{\partial z}=\xi S.$$

Shapiro and Willoughby showed solutions of the Sawyer-Eliassen equation for point sources (i.e. azimuthal rings) of heat and azimuthal momentum, based on the earlier work of Eliassen (1951). These solutions are reproduced in Fig. 2.12. The flow through the heat source follows a nearly vertical surface of constant absolute angular momentum, while that for a momentum source follows a nearly horizontal isentropic surface. For sources of heat and absolute angular momentum, the sense of the flow is upward and outward, respectively. For sinks the flow is reversed. The vortex axis lies to the left of the figure. In the warm-core system of panels (c) and (f), the warm anomaly that supports the slope of the constant absolute angular momentum and isentropic surfaces increases towards the upper left.

Shapiro and Willoughby used the Sawyer-Eliassen equation also to calculate the secondary circulation induced by point sources of heat and absolute angular momentum in balanced, tropical-cyclone-like vortices in a partially bounded domain using

the so-called method of images. Again they found that the secondary circulation through a heat source is primarily vertical, and that through a momentum source is primarily horizontal as shown in Fig. 2.13. The streamlines form two counter-rotating cells of circulation (or gyres) that extend outside the source. There is a strong flow between these gyres and a weaker return flow on the outside. The flow emerges from the source, spreads outward through a large volume surrounding it, and converges back into it from below. Thus, compensating subsidence surrounds heat-induced updraughts and compensating inflow lies above and below momentum-induced outflow. The horizontal scale of the gyres is just the local Rossby radius of deformation, so that the ratio of horizontal to vertical scale is N/I.

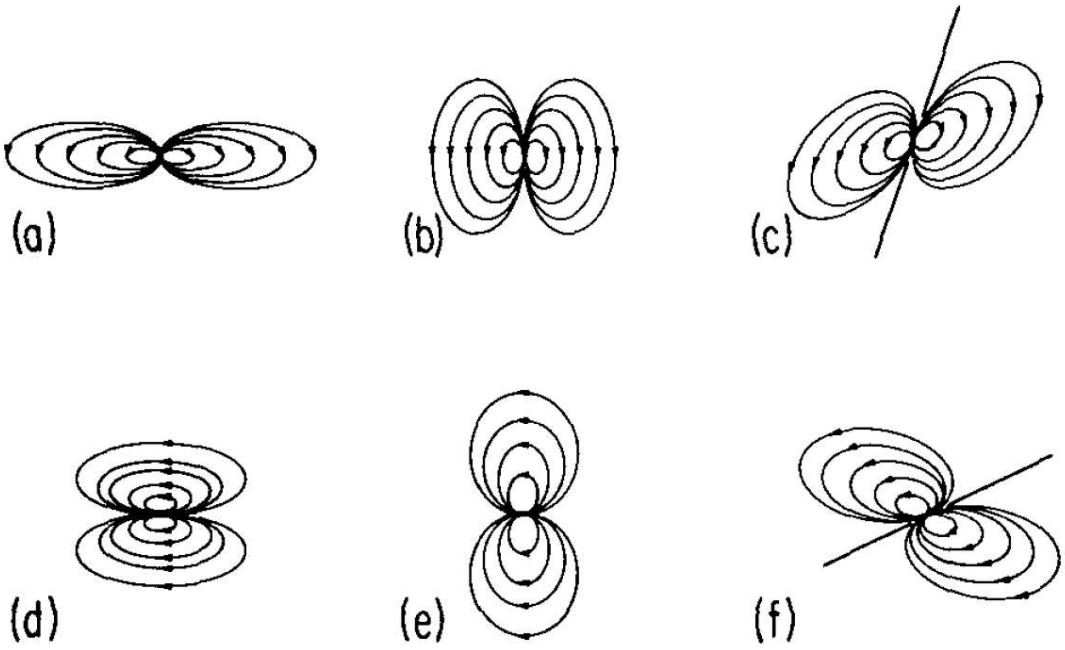

Figure 2.12: Streamfunction responses to point sources of: (a) Heat in a barotropic vortex with weak inertial stability, (b) heat in a barotropic vortex with strong inertial stability, (c) heat in a baroclinic vortex, (d) momentum in a barotropic vortex with weak inertial stability, (e) momentum in a barotropic vortex with strong inertial stability, and (f) momentum in a baroclinic vortex. (Based on Figs. 8, 9, 11, and 12 of Eliassen, (1951).)

Radial gradients of absolute angular momentum of the primary circulation affect the radial scale of the dipoles just as the static stability affects their vertical scale. For a fixed static stability, the gyres tend to be elongated vertically when the inertial-stability parameter I^2 is large and elongated horizontally when I^2 is small. Vertical gradients of absolute angular momentum associated with the vertical shear of the primary circulation tilt the updraught through a heat source because the path of least resistance for the rising air lies along surfaces of constant absolute angular

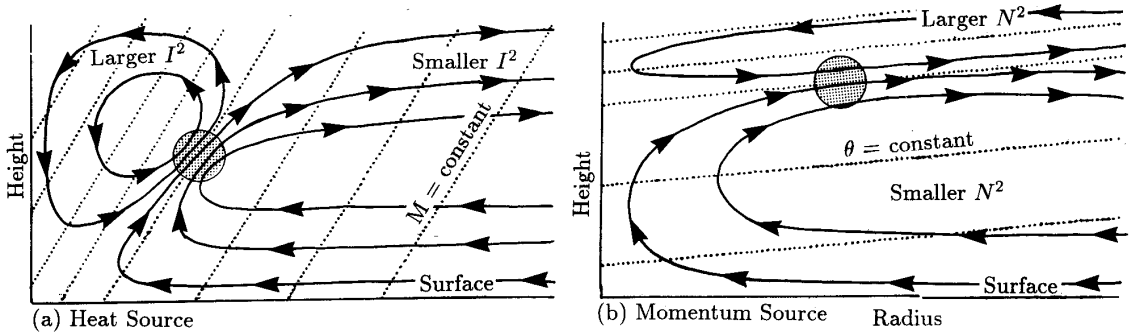

Figure 2.13: Secondary circulation induced in a balanced vortex by (a) a heat source and (b) a cyclonic momentum source showing the distortion induced by variation in inertial stability, I^2 and thermodynamic stability. N^2, and baroclinicity S^2. The strong motions through the source follow lines of constant angular momentum for a heat source and of constant potential temperature for a momentum source. From Willoughby (1995).

momentum. Likewise, horizontal temperature gradients associated with the vertical shear deflect the flow through momentum sources from the horizontal because the path of least resistance in this case lies along isentropic surfaces. Although the flow associated with a heat (momentum) source lies generally along the M-surface (θ-surface), it does have a small component across this surface. It is the advection by this component that causes evolution of the primary circulation. It can be shown that the swirling flow remains in approximate gradient-wind balance provided the time scale of the forcing is longer than the orbital period of the primary circulation about the vortex centre.

It turns out that the induced secondary circulation in balanced flows tend to cancel the direct effect of forcing. For example, the work done by expansion in the updraught induced by a heat source nearly balances the actual heating so that the increase in temperature is relatively small. Similarly, a momentum source produces outflow that advects compensating low values of absolute angular momentum from the central region of the vortex.

In section 2.15 we show how the Sawyer-Eliassen equation can be used as one of a set of equations to calculate the evolution of a balanced vortex.

2.14.1 Ertel PV and the discriminant

I show now that D is proportional to the the Ertel potential vorticity is defined as

$$P = \frac{(\omega + \mathbf{f}) \cdot \nabla\theta}{\rho}.$$

For a symmetric vortex with tangential wind speed distribution $v(r,z)$, $\omega + \mathbf{f} = -(\partial v/\partial z)\hat{\mathbf{r}} + (\zeta + f)\hat{\mathbf{z}}$ and $\nabla\theta = -(1/\chi^2)\nabla\chi = -\theta^2[(\partial\chi/\partial r)\hat{\mathbf{r}} + (\partial\chi/\partial z)\hat{\mathbf{z}}]$ so that

$$P = \frac{\theta^2}{\rho}\left[\frac{\partial v}{\partial z}\frac{\partial \chi}{\partial r} - (\zeta + f)\frac{\partial \chi}{\partial z}\right]$$

Then

$$\frac{g\rho\chi\xi}{\theta^2}P = -g\frac{\partial\chi}{\partial z}\xi\chi(\zeta + f) + \xi S\chi g\frac{\partial\chi}{\partial r}$$

or

$$\frac{g\rho\chi\xi}{\theta^2}P = -g\frac{\partial\chi}{\partial z}\left[\chi\xi(\zeta + f) + C\frac{\partial\chi}{\partial r}\right] + g\frac{\partial\chi}{\partial z}C\frac{\partial\chi}{\partial r} + \chi\frac{\partial C}{\partial z}g\frac{\partial\chi}{\partial r}$$

or

$$\frac{g\rho\chi\xi}{\theta^2}P = -g\frac{\partial\chi}{\partial z}\left[\chi\xi(\zeta + f) + C\frac{\partial\chi}{\partial r}\right] + g\frac{\partial\chi}{\partial r}\frac{\partial}{\partial z}(C\chi)$$

Finally

$$\frac{g\rho\chi\xi}{\theta^2}P = -g\frac{\partial\chi}{\partial z}\left[\chi\xi(\zeta + f) + C\frac{\partial\chi}{\partial r}\right] - \left(\frac{\partial}{\partial z}(C\chi)\right)^2$$

i.e.

$$\frac{g\rho\xi}{\theta^3}P = D \tag{2.95}$$

2.14.2 The forcing term for ψ in terms of generalized buoyancy

Consider the forcing term for Eq. (2.94). The term can be written:

$$F = -g\frac{\partial}{\partial r}\left(\frac{1}{\theta^2}\frac{d\theta}{dt}\right) - \frac{\partial}{\partial z}\left(C\frac{1}{\theta^2}\frac{d\theta}{dt}\right)$$

The generalized buoyancy (Eq. 2.78) is $\mathbf{b_e} = \mathbf{g_e}(\theta - \theta_e)/\theta_e$, where $\mathbf{g_e} = (C, 0, -g)$. With the anelastic approximation that $1/\theta \approx 1/\theta_e \approx 1/\Theta$, where Θ is some vertically averaged value of θ_e we have that

$$\frac{d\mathbf{b_e}}{dt} \approx \frac{1}{\Theta}\frac{d\theta}{dt}\mathbf{g_e}$$

Now

$$\hat{\theta}\cdot\nabla\wedge\frac{d\mathbf{b_e}}{dt} = \frac{\partial}{\partial r}\left(\frac{db_{ez}}{dt}\right) - \frac{\partial}{\partial z}\left(\frac{db_{er}}{dt}\right) \approx \frac{\partial}{\partial r}\left(\frac{g}{\Theta}\frac{d\theta}{dt}\right) - \frac{\partial}{\partial z}\left(\frac{C}{\Theta}\frac{d\theta}{dt}\right)$$

so that

$$F \approx \frac{1}{\Theta}\hat{\theta}.\nabla\wedge\frac{d\mathbf{b_e}}{dt} \tag{2.96}$$

2.14.3 The Sawyer-Eliassen equation and toroidal vorticity equation

The Sawyer-Eliassen equation is an approximate form of the local time derivative of equation for the toroidal vorticity $\eta = \partial u/\partial z - \partial w/\partial r$. Assuming the most general form of the continuity equation

$$\frac{\partial \rho}{\partial t} + \frac{1}{r}\frac{\partial}{\partial r}(r\rho u) + \frac{\partial}{\partial z}(\rho w) = 0$$

the toroidal vorticity equation may be written as

$$r\frac{D}{Dt}\left(\frac{\eta}{r\rho}\right) = \frac{1}{\rho}\frac{\partial C}{\partial z} + \frac{1}{\rho^2\chi}\left(\frac{\partial \chi}{\partial r}\frac{\partial p}{\partial z} - \frac{\partial \chi}{\partial z}\frac{\partial p}{\partial r}\right) \tag{2.97}$$

where $D/Dt \equiv \partial/\partial t + \mathbf{u}\cdot\nabla$ and $\eta/(r\rho)$ is a 'potential toroidal vorticity', where the analogous 'depth' is 'r', the radius of a toroidal vortex ring. If thermal wind balance exists, the right-hand-side of (**??**) may be written as

$$-\frac{1}{\rho\chi}\left(g\frac{\partial \chi}{\partial r} + \frac{\partial}{\partial z}(C\chi)\right).$$

Then the time derivative of (2.97) is

$$\frac{\partial}{\partial t}\left[r\frac{D}{Dt}\left(\frac{\eta}{r\rho}\right)\right] = -\frac{\partial}{\partial t}\left[\frac{1}{\rho\chi}\left(g\frac{\partial \chi}{\partial r} + \frac{\partial}{\partial z}(C\chi)\right)\right] \tag{2.98}$$

The right-hand-side of (2.98) gives the Sawyer-Eliassen equation when the thermal wind equation (2.14) is satisfied for all time. Then consistency requires that the left-hand-side is identically zero.

2.14.4 Buoyancy relative to a balanced vortex

Tropical cyclones are rapidly-rotating warm-cored vortices and the warm core is therefore positively buoyant relative to the environment. On the cyclone scale, however, hydrostatic and gradient-wind balance exist to a good approximation (Willoughby 1990) and the radial density (or buoyancy) gradient is related by the thermal-wind equation to the decay in the mean tangential circulation and density with height (see e.g. Smith 1980). Clearly much of the radial gradient of buoyancy force cannot be thought of as being "available" for driving a secondary (or toroidal) circulation of the vortex that is necessary for vortex amplification. Nevertheless, hydrostatic balance may be a poor approximation in individual convective clouds and a pertinent question is whether these clouds have significant local (unbalanced) buoyancy, which in turn might play an important role in the dynamics of storm intensification. This important question was addressed by Braun (2002), who answered it in the affirmative on the basis of his simulations of Hurricane Bob (1991). To address this question

it is necessary to define the perturbation pressure and perturbation density relative to some vortex-scale pressure and density distributions. The simplest case is when the primary vortex is approximately steady and axisymmetric. Then we may take reference distributions $p_0(r,z)$ and $\rho_0(r,z)$, respectively, that are in thermal wind balance with the tangential flow field $v_0(r,z)$. The thermal wind equation gives:

$$\frac{g}{\rho_0}\frac{\partial \rho_0}{\partial r} + \left(\frac{v_0^2}{r} + f v_0\right)\frac{1}{\rho_0}\frac{\partial \rho_0}{\partial z} = -\left(\frac{2v_0}{r} + f\right)\frac{\partial v_0}{\partial z}. \tag{2.99}$$

This is a linear first-order partial differential equation for $\ln(\rho_0/\rho_a)$, the characteristics of which satisfy

$$\frac{dz}{dr} = \frac{1}{g}\left(\frac{v_0^2}{r} + f v_0\right). \tag{2.100}$$

It is easy to show that these characteristics are just the isobaric surfaces [5] and the density variation along them is governed by the equation

$$\frac{d}{dr}\ln\left(\frac{\rho_0}{\rho_a}\right) = -\frac{1}{g}\left(\frac{2v_0}{r} + f\right)\frac{\partial v_0}{\partial z}. \tag{2.101}$$

Given the vertical density profile, $\rho_a(z)$, at some radius R, these equations can be integrated inwards along the isobars to obtain the balanced axisymmetric density and pressure distributions. We may use $\rho_0(r,z)$ and $p_0(r,z)$ as alternative reference quantities to define the buoyancy force in Eq. (2.10) (similar to Braun 2002), without affecting the derivation of this equation. We denote the generalized buoyancy force so calculated by $\mathbf{b_B}$. It follows that $\mathbf{b_B} \equiv \mathbf{0}$ in the axisymmetric balanced state, whereas, if the reference pressure and density at $r = R$ are used, $\mathbf{b}$ equals some nonzero function $\mathbf{b_0}(r,z)$. Clearly, the partition of force between perturbation pressure gradient and buoyancy will be different for the reference state characterized by $\rho_0(r,z)$ and $p_0(r,z)$ and interpretations of the dynamics will be different also, albeit equivalent to those using the more conventional reference quantities that depend on height only.

In the more general case, when the vortex structure has marked asymmetries and/or is evolving in time, it is necessary to allow for the azimuthal and/or time variations of the reference state as was done by Zhang *et al.* (2000) and Braun (2002).

2.14.5 Buoyancy in axisymmetric balanced vortices

Axisymmetric balanced models of tropical cyclone intensification (e.g. Ooyama, 1969) appear to capture many important observed features of tropical cyclone behaviour. However, in an axisymmetric model that assumes exact thermal wind balance,

[5] A small displacement (dr, dz) along an isobaric surface satisfies $(\partial p_0/\partial r)dr + (\partial p_0/\partial z)dz = 0$. Using the equations for hydrostatic balance, $\partial p_0/\partial z = -g\rho_0$, and gradient wind balance, $\partial p_0/\partial r = \rho_0(v^2/r + fv)$, gives the equation for the characteristics.

$\mathbf{b_B}(r,z,t) \equiv \mathbf{0}$ and the corresponding $\partial p'/\partial z \equiv 0$, even though there may be heat sources or sinks present that generate buoyancy $\mathbf{b}$. It is clear from the foregoing discussion that any diabatic heating or cooling in such models is incorporated directly into the balanced state, changing $\mathbf{b}(r,z,t)$, while $\mathbf{b_B}(r,z,t)$ remains identically zero by definition. Obviously, nonzero values of $\mathbf{b_B}$ relate to *unbalanced motions* provided that the appropriate reference state as defined above has been selected for the definition of buoyancy at any given time. It may be helpful to think of $\mathbf{b}$ as characterizing the *system buoyancy* and $\mathbf{b_B}$ as characterizing the *local buoyancy*.

2.15 Origins of buoyancy in tropical cyclones

Tropical cyclones intensify when, as a direct or indirect result of latent heat release, the buoyancy b in the core increases. To a first approximation, the direct effect of latent heat release in saturated ascending air, such as in the eyewall clouds, or in the cores of individual convective clouds, is to maintain the air close to the moist adiabat from which the updraught originates. The indirect effect of latent heat release is to produce subsidence (or at least reduce the rate-of-ascent) in clear-air regions adjacent to (i.e. within a local Rossby radius of deformation of) deep convection. There is observational evidence (e.g. Betts, 1986; Xu and Emanuel, 1992) and evidence from model studies (Bretherton and Smolarkewicz, 1989) that, again to a first approximation, the clear air properties are adjusted towards the same saturation moist adiabat as in the neighbouring convective cores, albeit in this case to one calculated reversibly. In either case, the thermal structure of the troposphere in a mature tropical cyclone, and thereby the radial distribution of buoyancy, would be determined largely by the radial distribution of moist entropy at the top of the subcloud layer, at least in regions of ascent (see e.g. Emanuel, 1991). This view relates essentially to the generation of system buoyancy.

The extent to which local (unbalanced) buoyancy is produced will depend amongst other things on the rate at which the buoyancy is generated and the scale on which it is generated. For example, the simulations by Braun (2002) indicate that much of the eyewall updraft mass flux occurs within small-scale updrafts that are locally buoyant relative to the broad-scale thermal field of the vortex. A recent examination of the high resolution cloud resolving numerical simulation of the formation of Hurricane Diana (1984) has shown how buoyant cores growing in the rotation-rich environment of an incipient storm produce intense cyclonic vorticity anomalies in the lower troposphere by vortex-tube stretching (Hendricks, *et al.* 2003). These intense vorticity anomalies subsequently merge and axisymmetrize to intensify the balanced circulation of the incipient mesoscale vortex (Montgomery and Enagonio 1998; Möller and Montgomery 2000; Montgomery and Brunet 2002). In this case, subsidence warming is not the primary means for generating the cyclone's warm core. Rather, the warm core temperature that materializes within the developing mesoscale vortex results from the tendency of the high vorticity cores of the buoyant plumes to 'trap' the heat releases by the condensation process, as one might antici-

pate from local Rossby adjustment considerations (Schubert *et al.* 1980, Sec. 9) and quasi-balanced dynamics within enhanced vortical regions (Schubert and Hack 1982, Montgomery *et al.* 2003).

2.16 A balanced theory of vortex evolution

The establishment of the Sawyer-Eliassen equation is an important step in formulating a balanced theory for the evolution of an axisymmetric vortex. In such a theory we need prognostic equations for the evolution of the primary circulation, i.e. for the azimuthal wind and potential temperature. These are just the axisymmetric forms of Eqs. (2.2) and (2.5), i.e. Eqs. (2.90) and (2.91). Given expressions for $\dot{V}$ and $\dot{\theta}$ and initial conditions for v and θ, we can solve the Sawyer-Eliassen equation for the streamfunction of the secondary circulation, ψ, given suitable boundary conditions on this quantity. This streamfunction gives the secondary circulation that keeps v and θ in thermal-wind balance for short time interval, Δt. The corresponding radial and vertical wind components may be obtained from the expressions (2.89) and the density therein can be obtained from ???

complete

2.17 Appendices to Chapter 2

2.17.1 Maxwell's Equations

In a saturated atmosphere it is possible to define a saturated moist entropy, s^*, which is invariant under moist reversible processes. This quantity satisfies a modified form of the first law of thermodynamics:

$$Tds^* = du + pda - Ldq^*, \tag{2.102}$$

where u is the internal energy, L is the heat of vaporization, and q^* is the saturation mixing ratio. It is also possible to define a saturated moist enthalpy h^* such that

$$h^* - u + pa - Lq^*. \tag{2.103}$$

From (2.102) and (2.103) it follows that

$$dh^* = Tds^* + \alpha dp. \tag{2.104}$$

From this it may be deduced that

$$\left(\frac{\partial h^*}{\partial p}\right)_{s^*} = \alpha \tag{2.105}$$

$$\left(\frac{\partial h^*}{\partial s^*}\right)_{p} = T. \tag{2.106}$$

Now, because q^* is a function of temperature and pressure alone, h^* is a state variable which may be expressed as a function of any other two state variables, such as p and s^*. Thus

$$\left(\frac{\partial h^*}{\partial s^*}\right)_p \left(\frac{\partial h^*}{\partial p}\right)_{s^*} = \left(\frac{\partial h^*}{\partial p}\right)_{s^*} \left(\frac{\partial h^*}{\partial s^*}\right)_p \tag{2.107}$$

Substituting (2.105) and (2.106) into the above we obtain

$$\left(\frac{\partial \alpha}{\partial s^*}\right)_p = \left(\frac{\partial T}{\partial p}\right)_{s^*} \tag{2.108}$$

which is the desired result.